

# Density Model for Mesoplodont Beaked Whales (*Mesoplodon spp.*) for the U.S. East Coast: Supplementary Report

Model Version 7.1

Duke University Marine Geospatial Ecology Laboratory\*

2023-05-27


## Citation

When citing our methodology or results generally, please cite Roberts et al. (2016, 2023). The complete references appear at the end of this document. We are preparing a new article for a peer-reviewed journal that will eventually replace those. Until that is published, those are the best general citations.

When citing this model specifically, please use this reference:

Roberts JJ, Yack TM, Cañadas A, Fujioka E, Halpin PN, Barco SG, Boisseau O, Chavez-Rosales S, Cole TVN, Cotter MP, Cummings EW, Davis GE, DiGiovanni Jr. RA, Garrison LP, Gowan TA, Jackson KA, Kenney RD, Khan CB, Lockhart GG, Lomac-MacNair KS, McAlarney RJ, McLellan WA, Mullin KD, Nowacek DP, O'Brien O, Pabst DA, Palka DL, Quintana-Rizzo E, Redfern JV, Rickard ME, White M, Whitt AD, Zoidis AM (2022) Density Model for Mesoplodont Beaked Whales (*Mesoplodon spp.*) for the U.S. East Coast, Version 7.1, 2023-05-27, and Supplementary Report. Marine Geospatial Ecology Laboratory, Duke University, Durham, North Carolina.

## Copyright and License

 This document and the accompanying results are © 2023 by the Duke University Marine Geospatial Ecology Laboratory and are licensed under a [Creative Commons Attribution 4.0 International License](https://creativecommons.org/licenses/by/4.0/).

## Model Version History

---

Version	Date	Description
5	2017-06-01	Began update to Roberts et al. (2015) models. Introduced new surveys from AMAPPS, NARWSS, UNCW, VAMSC, and the SEUS NARW teams. Updated modeling methodology. Refitted detection functions. Split Roberts et al. (2015) beaked whale guild into three taxa: Cuvier's beaked whale, the Mesoplodont guild, and unidentified beaked whales. Fit new spatial models from scratch using new and reprocessed covariates.
6	2017-08-10	Removed biological predictors, reintroduced pre-1998 data, and refitted models. These predictors cause extreme extrapolations of high density offshore in April and May in unsurveyed waters. Model released as part of a scheduled update to the U.S. Navy Marine Species Density Database (NMSDD).

---

\*For questions or to offer feedback please contact Jason Roberts ([jason.roberts@duke.edu](mailto:jason.roberts@duke.edu)) and Tina Yack ([tina.yack@duke.edu](mailto:tina.yack@duke.edu))

*(continued)*

---

Version	Date	Description
7	2022-06-20	This model is a major update over the prior version, with substantial additional data, improved statistical methods, and an increased spatial resolution. It was released as part of the final delivery of the U.S. Navy Marine Species Density Database (NMSDD) for the Atlantic Fleet Testing and Training (AFTT) Phase IV Environmental Impact Statement. Several new collaborators joined and contributed survey data: New York State Department of Environmental Conservation, TetraTech, HDR, and Marine Conservation Research. We incorporated additional surveys from all continuing and new collaborators through the end of 2020. (Because some environmental covariates were only available through 2019, certain models only extend through 2019.) We increased the spatial resolution to 5 km and, at NOAA's request, we extended the model further inshore from New York through Maine. We reformulated and refitted all detection functions and spatial models. We updated all environmental covariates to newer products, when available, and added several covariates to the set of candidates. For models that incorporated dynamic covariates, we estimated model uncertainty using a new method that accounts for both model parameter error and temporal variability.
7.1	2023-05-27	Completed the supplementary report documenting the details of this model. The model itself was not changed.

---

# 1 Survey Data

We built this model from data collected between 2010-2019 (Table 1, Figure 1). In keeping with our primary strategy for the 2022 modeling cycle, we excluded data prior to 1998 in order to utilize biological covariates derived from satellite ocean color observations, which were only available for a few months before 1998. However, given that there were only 35 observations of Mesoplodont beaked whales prior to 2010 and improvements were made to species identification starting in 2010, we elected to exclude data prior to 2010. We also excluded data after 2019 in order to utilize zooplankton and micronekton biomass estimates from SEAPODYM (Lehodey et al. 2008), which preliminary modeling indicated were effective spatial covariates but were only available through 2019. Further, we excluded surveys that did not include beaked whales within their list of target species. We restricted the model to survey transects with sea states of Beaufort 5 or less (for a few surveys we used Beaufort 4 or less) for both aerial and shipboard surveys. We also excluded transects with poor weather or visibility for surveys that reported those conditions.

Table 1: Survey effort and observations considered for this model. Effort is tallied as the cumulative length of on-effort transects. Observations are the number of groups and individuals encountered while on effort. Off effort observations and those lacking an estimate of group size or distance to the group were excluded.

Institution	Program	Period	Effort	Observations		
			1000s km	Groups	Individuals	Mean Group Size
<b>Aerial Surveys</b>						
HDR	Navy Norfolk Canyon	2018-2019	11	2	9	4.5
NEAq	CNM	2017-2019	2	5	20	4.0
NEAq	MMS-WEA	2017-2019	31	0	0	
NEAq	NLPSC	2011-2015	43	0	0	
NEFSC	AMAPPS	2010-2019	89	0	0	
NEFSC	NARWSS	2010-2019	200	0	0	
NYS-DEC/TT	NYBWM	2017-2019	58	0	0	
SEFSC	AMAPPS	2010-2019	111	2	8	4.0
UNCW	Navy Cape Hatteras	2011-2017	34	29	75	2.6
UNCW	Navy Jacksonville	2010-2017	76	0	0	
UNCW	Navy Norfolk Canyon	2015-2017	14	2	5	2.5
UNCW	Navy Onslow Bay	2010-2011	14	3	10	3.3
VAMSC	MD DNR WEA	2013-2015	16	0	0	
VAMSC	Navy VACAPES	2016-2017	19	0	0	
VAMSC	VA CZM WEA	2012-2015	21	0	0	
		<b>Total</b>	<b>740</b>	<b>43</b>	<b>127</b>	<b>3.0</b>
<b>Shipboard Surveys</b>						
MCR	SOTW Acoustical	2019-2019	4	18	27	1.5
NEFSC	AMAPPS	2011-2016	14	109	318	2.9
SEFSC	AMAPPS	2011-2016	14	25	54	2.2
		<b>Total</b>	<b>33</b>	<b>152</b>	<b>399</b>	<b>2.6</b>
		<b>Grand Total</b>	<b>773</b>	<b>195</b>	<b>526</b>	<b>2.7</b>

Table 2: Institutions that contributed surveys used in this model.

Institution	Full Name
HDR	HDR, Inc.
MCR	Marine Conservation Research
NEAq	New England Aquarium
NEFSC	NOAA Northeast Fisheries Science Center
NYS-DEC/TT	New York State Department of Environmental Conservation and Tetra Tech, Inc.
SEFSC	NOAA Southeast Fisheries Science Center
UNCW	University of North Carolina Wilmington
VAMSC	Virginia Aquarium & Marine Science Center

Table 3: Descriptions and references for survey programs used in this model.

Program	Description	References
AMAPPS	Atlantic Marine Assessment Program for Protected Species	Palka et al. (2017), Palka et al. (2021)
CNM	Northeast Canyons Marine National Monument Aerial Surveys	Redfern et al. (2021)
MD DNR WEA	Aerial Surveys of the Maryland Wind Energy Area	Barco et al. (2015)
MMS-WEA	Marine Mammal Surveys of the MA and RI Wind Energy Areas	Quintana-Rizzo et al. (2021), O'Brien et al. (2022)
NARWSS	North Atlantic Right Whale Sighting Surveys	Cole et al. (2007)
Navy Cape Hatteras	Aerial Surveys of the Navy's Cape Hatteras Study Area	McLellan et al. (2018)
Navy Jacksonville	Aerial Surveys of the Navy's Jacksonville Study Area	Foley et al. (2019)
Navy Norfolk Canyon	Aerial Surveys of the Navy's Norfolk Canyon Study Area	Cotter (2019), McAlarney et al. (2018)
Navy Onslow Bay	Aerial Surveys of the Navy's Onslow Bay Study Area	Read et al. (2014)
Navy VACAPES	Aerial Survey Baseline Monitoring in the Continental Shelf Region of the VACAPES OPAREA	Mallette et al. (2017)
NLPSC	Northeast Large Pelagic Survey Collaborative Aerial Surveys	Leiter et al. (2017), Stone et al. (2017)
NYBWM	New York Bight Whale Monitoring Surveys	Zoidis et al. (2021)
SOTW Acoustical	R/V Song of the Whale Passive Acoustical Surveys	Boisseau et al. (in review)
VA CZM WEA	Virginia CZM Wind Energy Area Surveys	Mallette et al. (2014), Mallette et al. (2015)

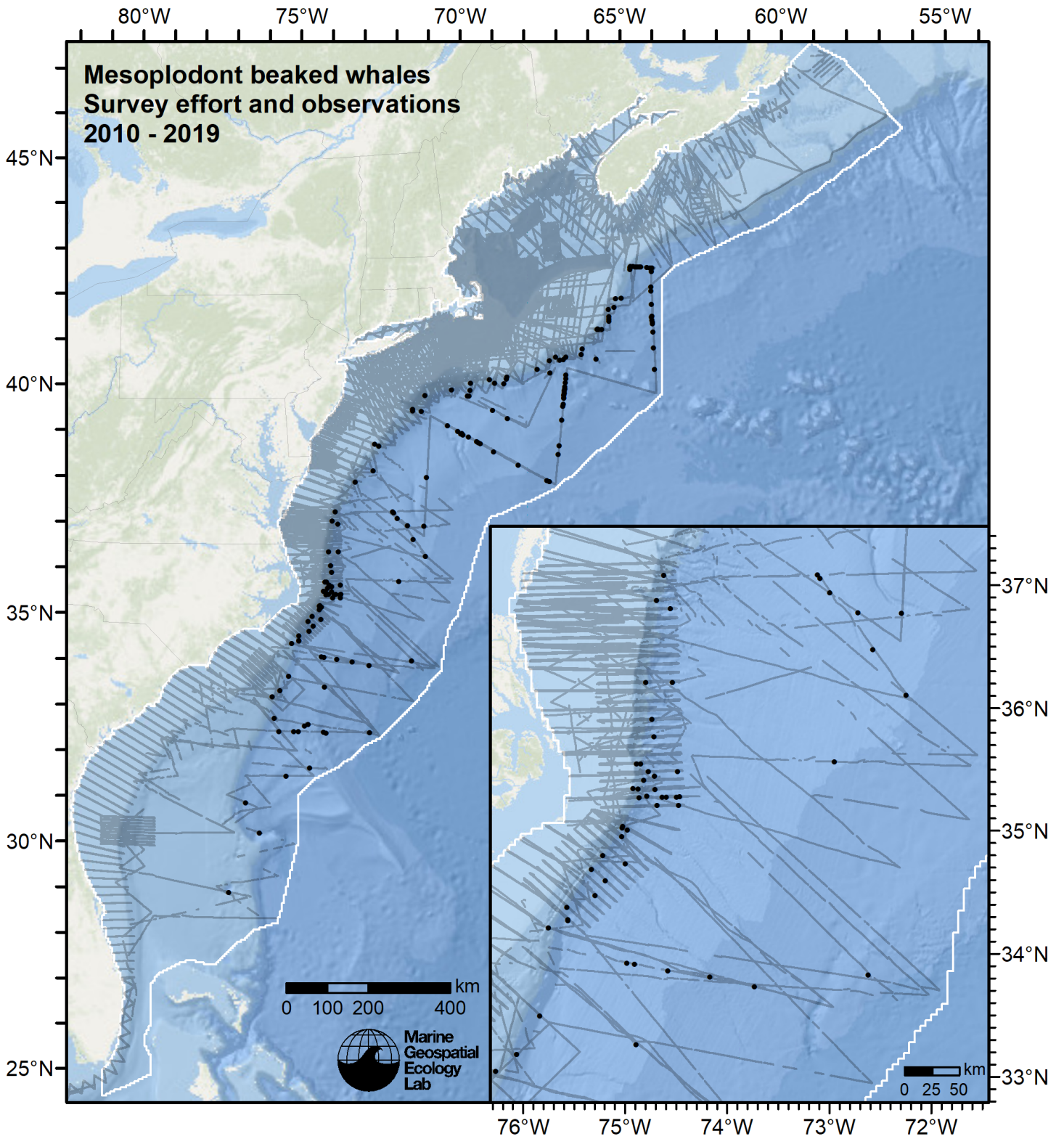


Figure 1: Survey effort and mesoplodont beaked whales observations available for density modeling, after detection functions were applied, and excluded segments and truncated observations were removed.

## 2 Detection Functions

### 2.1 With a Taxonomic Covariate

We fitted the detection functions in this section to pools of species with similar detectability characteristics and used the taxonomic identification as a covariate (ScientificName) to account for differences between them. We consulted the literature and observer teams to determine appropriate poolings. We usually employed this approach to boost the counts of observations in the detection functions, which increased the chance that other covariates such as Beaufort sea state could be used to account for differences in observing conditions. When defining the taxonomic covariate, we sometimes had too few observations of species to allocate each of them their own level of the covariate and had to group them together, again consulting the literature and observers for advice on species similarity. Also, when species were observed frequently enough to be allocated their own levels but statistical tests indicated no significant difference between the levels, we usually grouped them together into a single level.



### 2.1.1.1.1 600 ft

After right-truncating observations greater than 400 m, we fitted the detection function to the 109 observations that remained (Table 4). The selected detection function (Figure 3) used a hazard rate key function with OriginalScientificName (Figure 4) as a covariate.

Table 4: Observations used to fit the 600 ft detection function.

ScientificName	n
Hyperoodon ampullatus	3
Kogia	23
Mesoplodon	14
Mesoplodon bidens	1
Ziphiidae	33
Ziphius cavirostris	35
<b>Total</b>	<b>109</b>

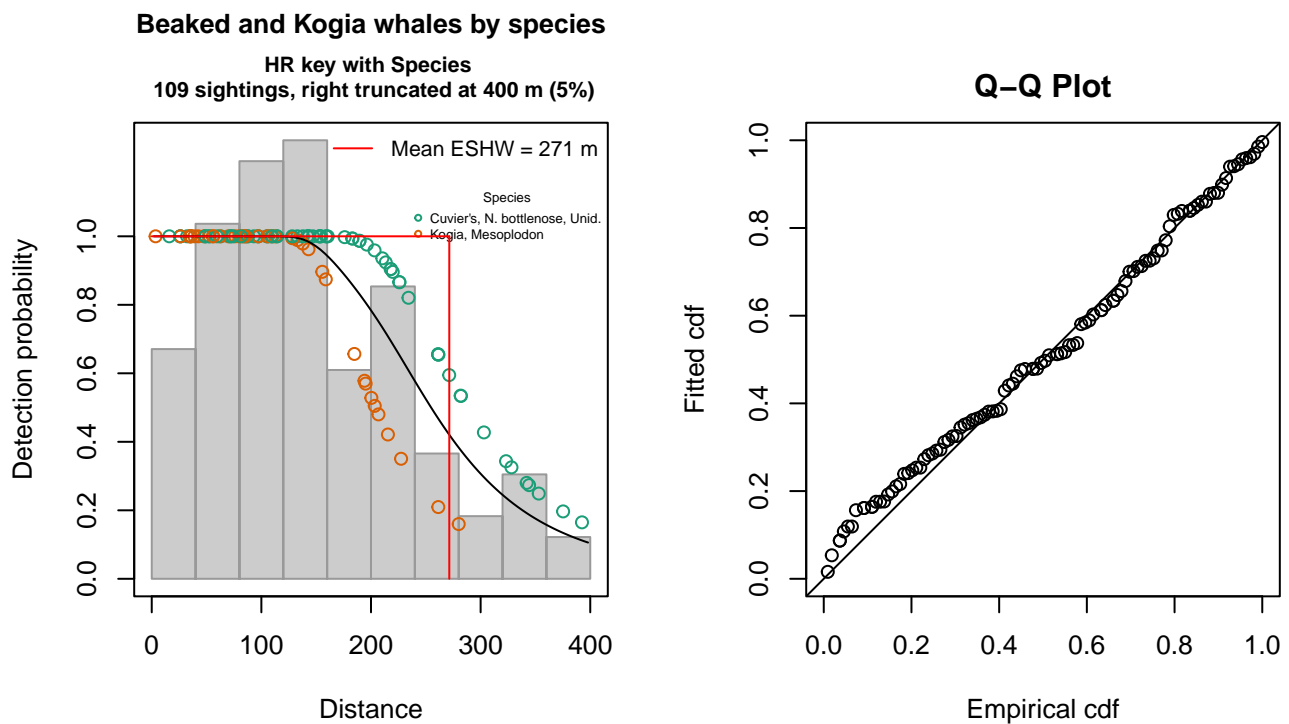


Figure 3: 600 ft detection function and Q-Q plot showing its goodness of fit.

Statistical output for this detection function:

Summary for ds object

Number of observations : 109  
 Distance range : 0 - 400  
 AIC : 1272.901

Detection function:

Hazard-rate key function

Detection function parameters

Scale coefficient(s):

	estimate	se
(Intercept)	5.5800164	0.1212472



OriginalScientificNameKogia, Mesoplodon -0.3454612 0.1492241

Shape coefficient(s):

	estimate	se
(Intercept)	1.474338	0.3977595

	Estimate	SE	CV
Average p	0.6645919	0.04555694	0.06854874
N in covered region	164.0104361	14.58154672	0.08890621

Distance sampling Cramer-von Mises test (unweighted)

Test statistic = 0.116256 p = 0.510907

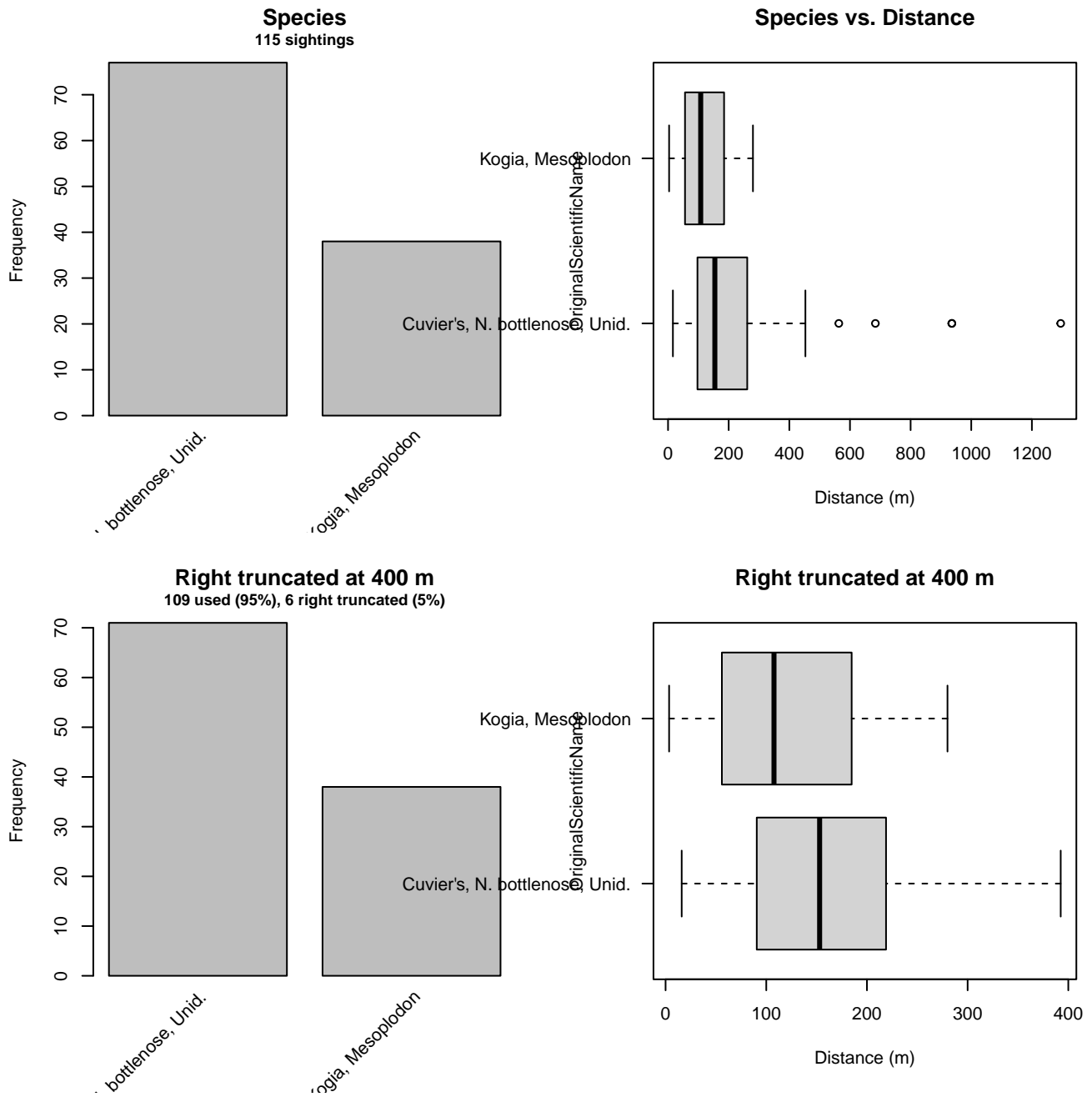


Figure 4: Distribution of the OriginalScientificName covariate before (top row) and after (bottom row) observations were truncated to fit the 600 ft detection function.

### 2.1.1.1.2 750 ft

After right-truncating observations greater than 1297 m, we fitted the detection function to the 80 observations that remained (Table 5). The selected detection function (Figure 5) used a hazard rate key function with Beaufort (Figure 6) and OriginalScientificName (Figure 7) as covariates.

Table 5: Observations used to fit the 750 ft detection function.

ScientificName	n
Kogia	55
Mesoplodon	9
Ziphiidae	12
Ziphius cavirostris	4
<b>Total</b>	<b>80</b>

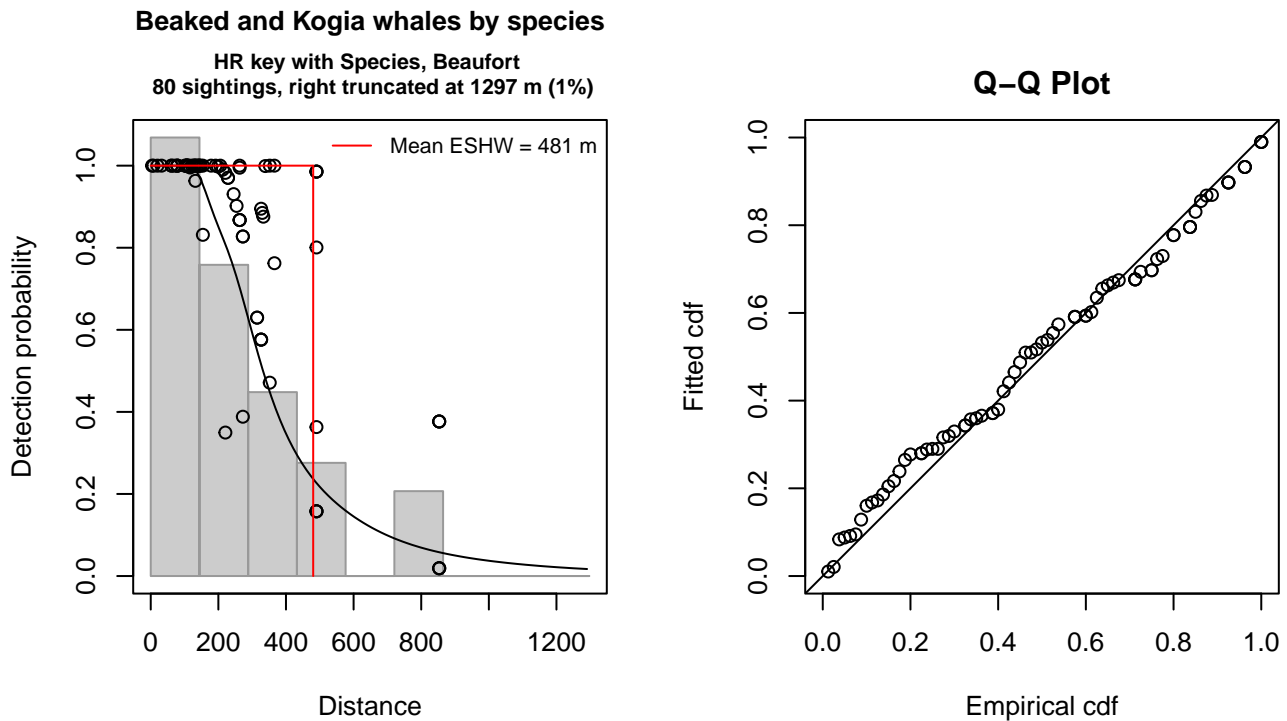


Figure 5: 750 ft detection function and Q-Q plot showing its goodness of fit.

Statistical output for this detection function:

Summary for ds object

Number of observations : 80  
 Distance range : 0 - 1297  
 AIC : 1037.791

Detection function:

Hazard-rate key function

Detection function parameters

Scale coefficient(s):

	estimate	se
(Intercept)	7.1253756	0.3142159
OriginalScientificNameKogia	-0.8097794	0.2203485
Beaufort	-0.5658239	0.1695498

Shape coefficient(s):

	estimate	se
(Intercept)	1.375855	0.1977036

	Estimate	SE	CV
Average p	0.3064062	0.03275229	0.1068917
N in covered region	261.0913218	37.74245080	0.1445565

Distance sampling Cramer-von Mises test (unweighted)  
Test statistic = 0.106921 p = 0.551997

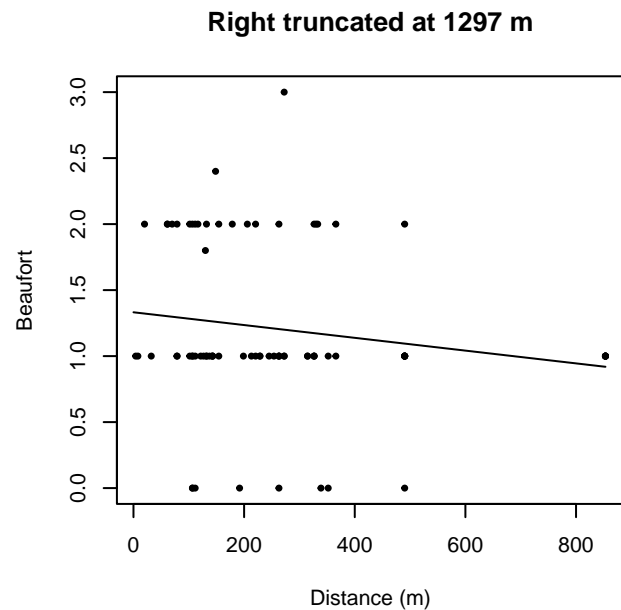
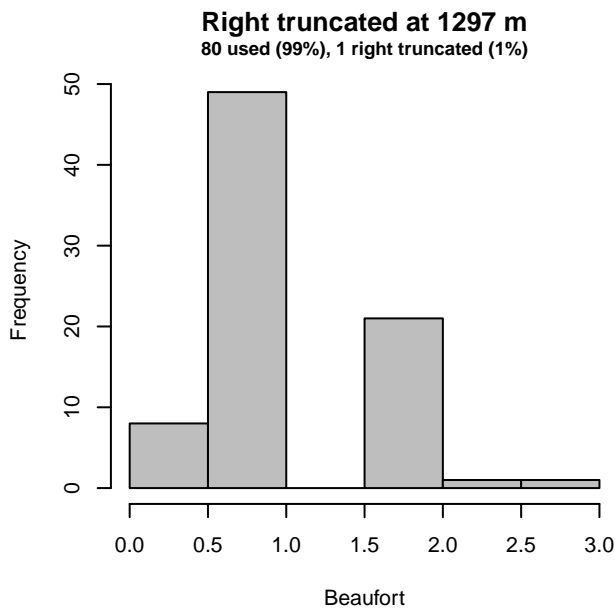
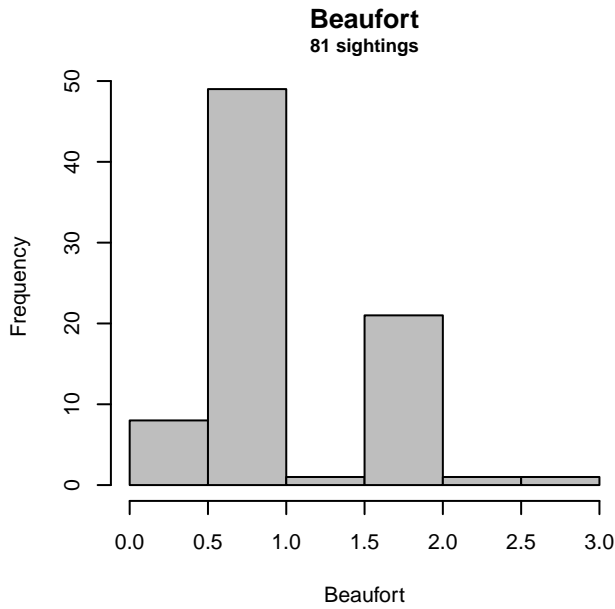


Figure 6: Distribution of the Beaufort covariate before (top row) and after (bottom row) observations were truncated to fit the 750 ft detection function.

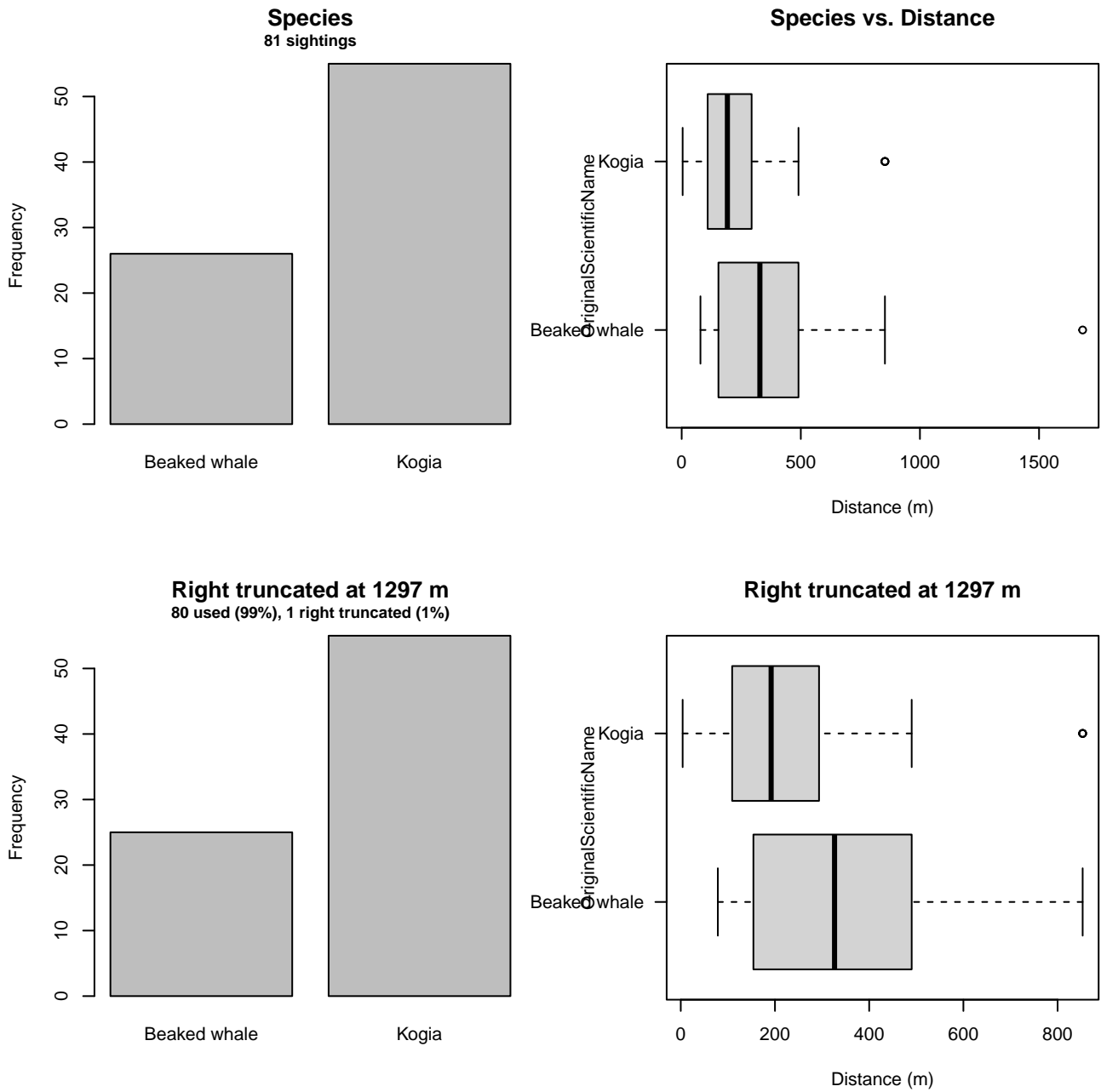


Figure 7: Distribution of the OriginalScientificName covariate before (top row) and after (bottom row) observations were truncated to fit the 750 ft detection function.

### 2.1.1.1.3 1000 ft

After right-truncating observations greater than 1250 m, we fitted the detection function to the 131 observations that remained (Table 6). The selected detection function (Figure 8) used a half normal key function with OriginalScientificName (Figure 9) as a covariate.

Table 6: Observations used to fit the 1000 ft detection function.

ScientificName	n
Hyperoodon ampullatus	1
Kogia	14
Kogia sima	1
Mesoplodon	26
Mesoplodon bidens	6
Mesoplodon europaeus	7
Mesoplodon mirus	3
Ziphiidae	11
Ziphius cavirostris	62
<b>Total</b>	<b>131</b>

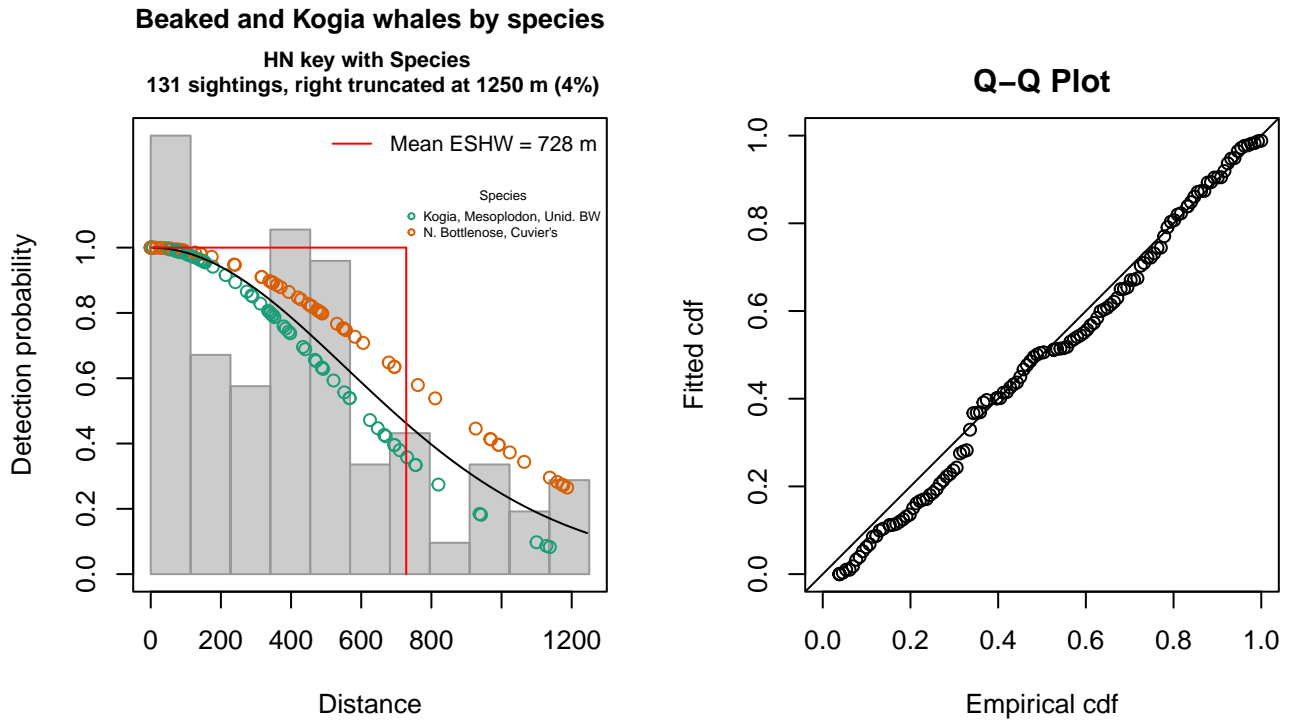


Figure 8: 1000 ft detection function and Q-Q plot showing its goodness of fit.

Statistical output for this detection function:

Summary for ds object

Number of observations : 131  
 Distance range : 0 - 1250  
 AIC : 1830.819

Detection function:

Half-normal key function

Detection function parameters

Scale coefficient(s):

	estimate	se
(Intercept)	6.2340705	0.1031336
OriginalScientificNameN. Bottlenose, Cuvier's	0.3570255	0.1899459

Estimate	SE	CV
----------	----	----

Average p 0.5712474 0.04000868 0.07003740  
 N in covered region 229.3227075 20.84792919 0.09091088

Distance sampling Cramer-von Mises test (unweighted)  
 Test statistic = 0.133457 p = 0.444164

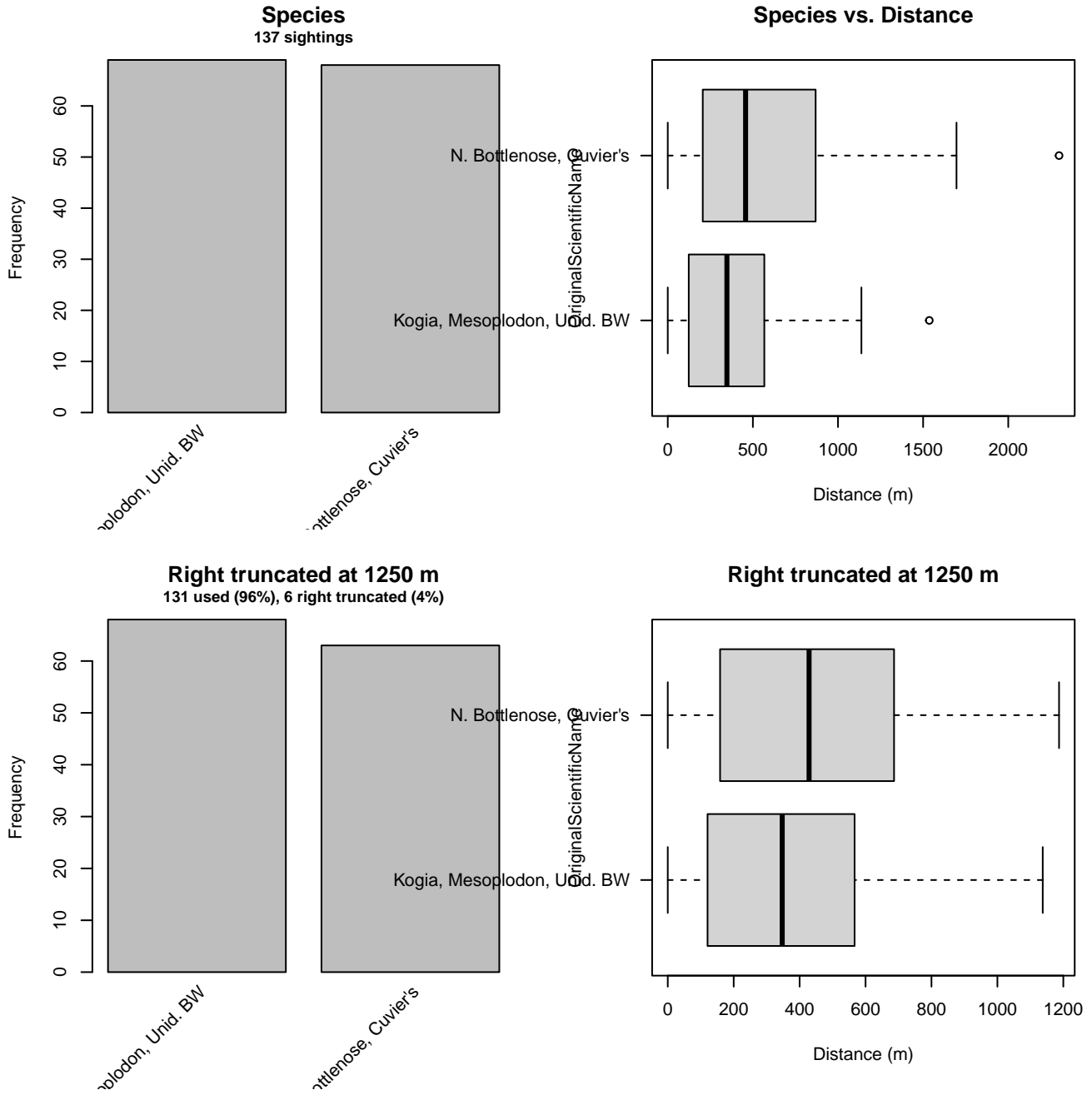


Figure 9: Distribution of the OriginalScientificName covariate before (top row) and after (bottom row) observations were truncated to fit the 1000 ft detection function.

### 2.1.1.2 Shipboard Surveys

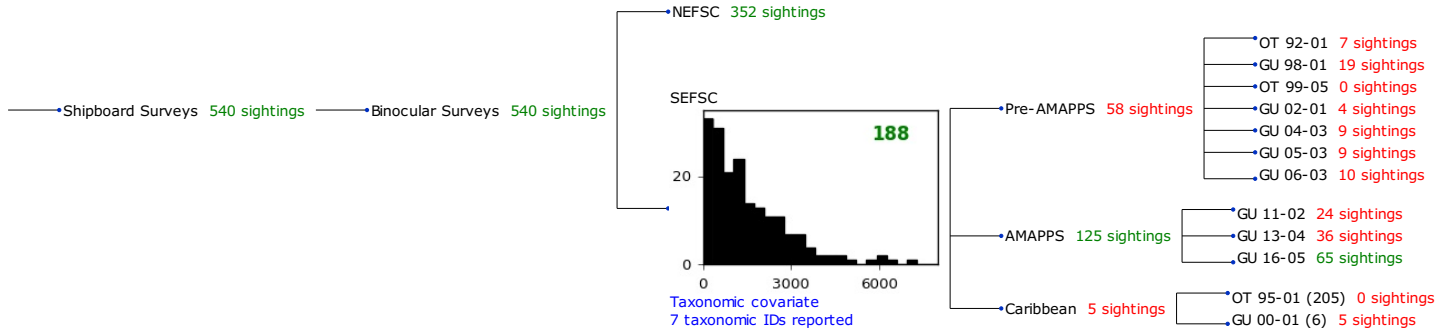


Figure 10: Detection hierarchy for shipboard surveys, showing how they were pooled during detectability modeling, for detection functions that pooled multiple taxa and used a taxonomic covariate to account for differences between them. Each histogram represents a detection function and summarizes the perpendicular distances of observations that were pooled to fit it, prior to truncation. Observation counts, also prior to truncation, are shown in green when they met the recommendation of Buckland et al. (2001) that detection functions utilize at least 60 sightings, and red otherwise. For rare taxa, it was not always possible to meet this recommendation, yielding higher statistical uncertainty. During the spatial modeling stage of the analysis, effective strip widths were computed for each survey using the closest detection function above it in the hierarchy (i.e. moving from right to left in the figure). Surveys that do not have a detection function above them in this figure were either addressed by a detection function presented in a different section of this report, or were omitted from the analysis.

#### 2.1.1.2.1 SEFSC

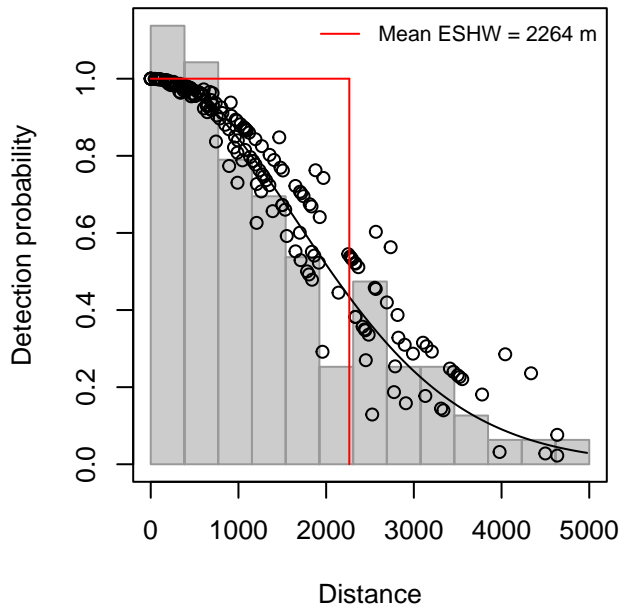
After right-truncating observations greater than 5000 m, we fitted the detection function to the 182 observations that remained (Table 7). The selected detection function (Figure 11) used a half normal key function with Beaufort (Figure 12) and OriginalScientificName (Figure 13) as covariates.

Table 7: Observations used to fit the SEFSC detection function.

ScientificName	n
Kogia	60
Kogia sima	9
Mesoplodon	37
Mesoplodon densirostris	3
Mesoplodon europaeus	1
Ziphiidae	52
Ziphius cavirostris	20
<b>Total</b>	<b>182</b>

### Beaked and Kogia whales by species

HN key with Species, Beaufort  
182 sightings, right truncated at 5000 m (3%)



### Q-Q Plot

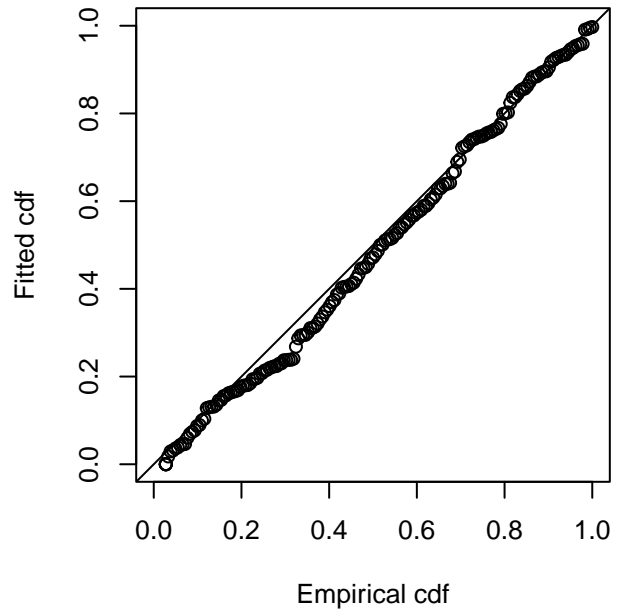


Figure 11: SEFSC detection function and Q-Q plot showing its goodness of fit.

Statistical output for this detection function:

Summary for ds object

Number of observations : 182  
Distance range : 0 - 5000  
AIC : 2985.886

Detection function:

Half-normal key function

Detection function parameters

Scale coefficient(s):

	estimate
(Intercept)	7.4282169
OriginalScientificNameMesoplodon spp. and Unid. beaked whale	0.1940795
OriginalScientificNameZiphius or N. bottlenose	0.4163007
Beaufort3-4	-0.2991956
	se
(Intercept)	0.08116764
OriginalScientificNameMesoplodon spp. and Unid. beaked whale	0.12604909
OriginalScientificNameZiphius or N. bottlenose	0.24124124
Beaufort3-4	0.13661134

	Estimate	SE	CV
Average p	0.4423162	0.02407533	0.05443013
N in covered region	411.4703239	32.09594942	0.07800307

Distance sampling Cramer-von Mises test (unweighted)

Test statistic = 0.128965 p = 0.460545



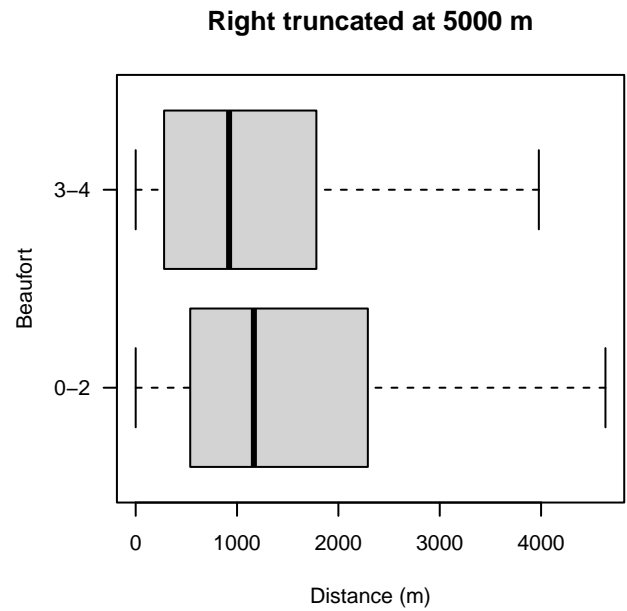
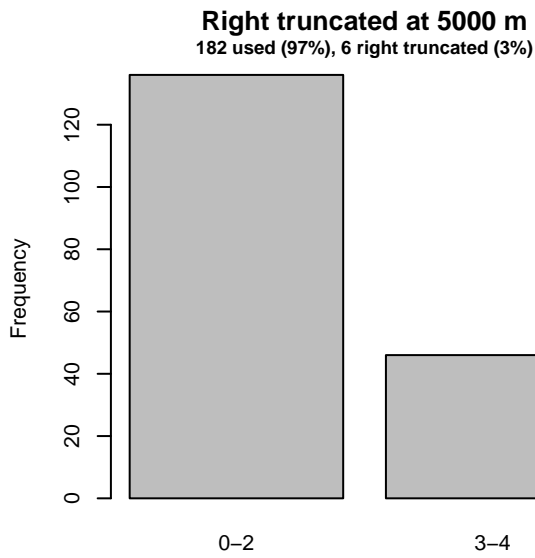
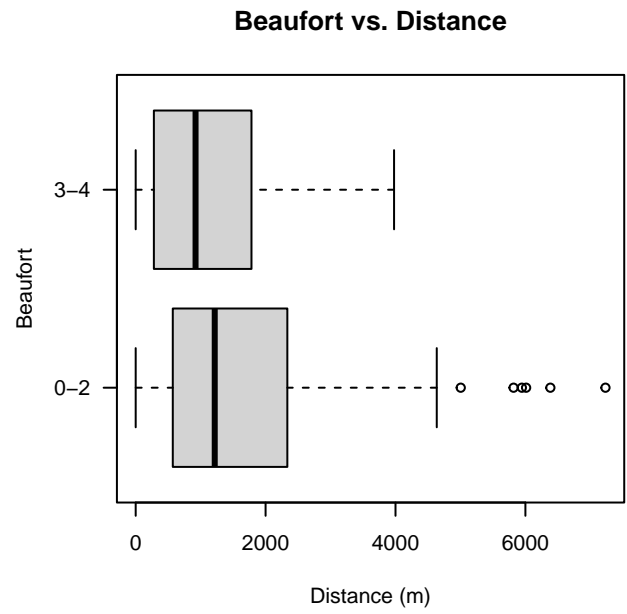
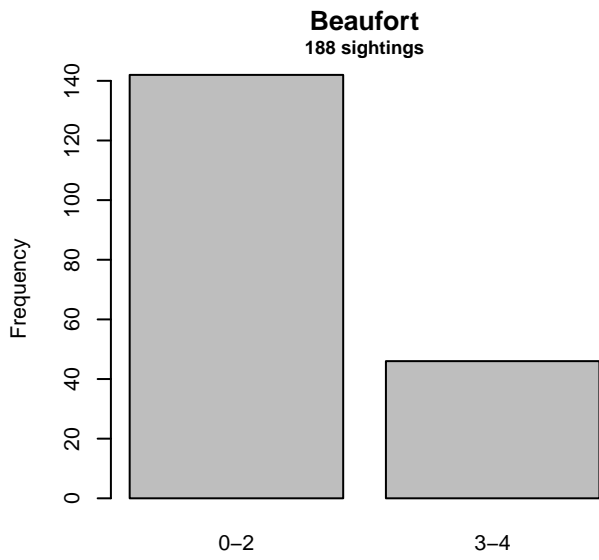


Figure 12: Distribution of the Beaufort covariate before (top row) and after (bottom row) observations were truncated to fit the SEFSC detection function.

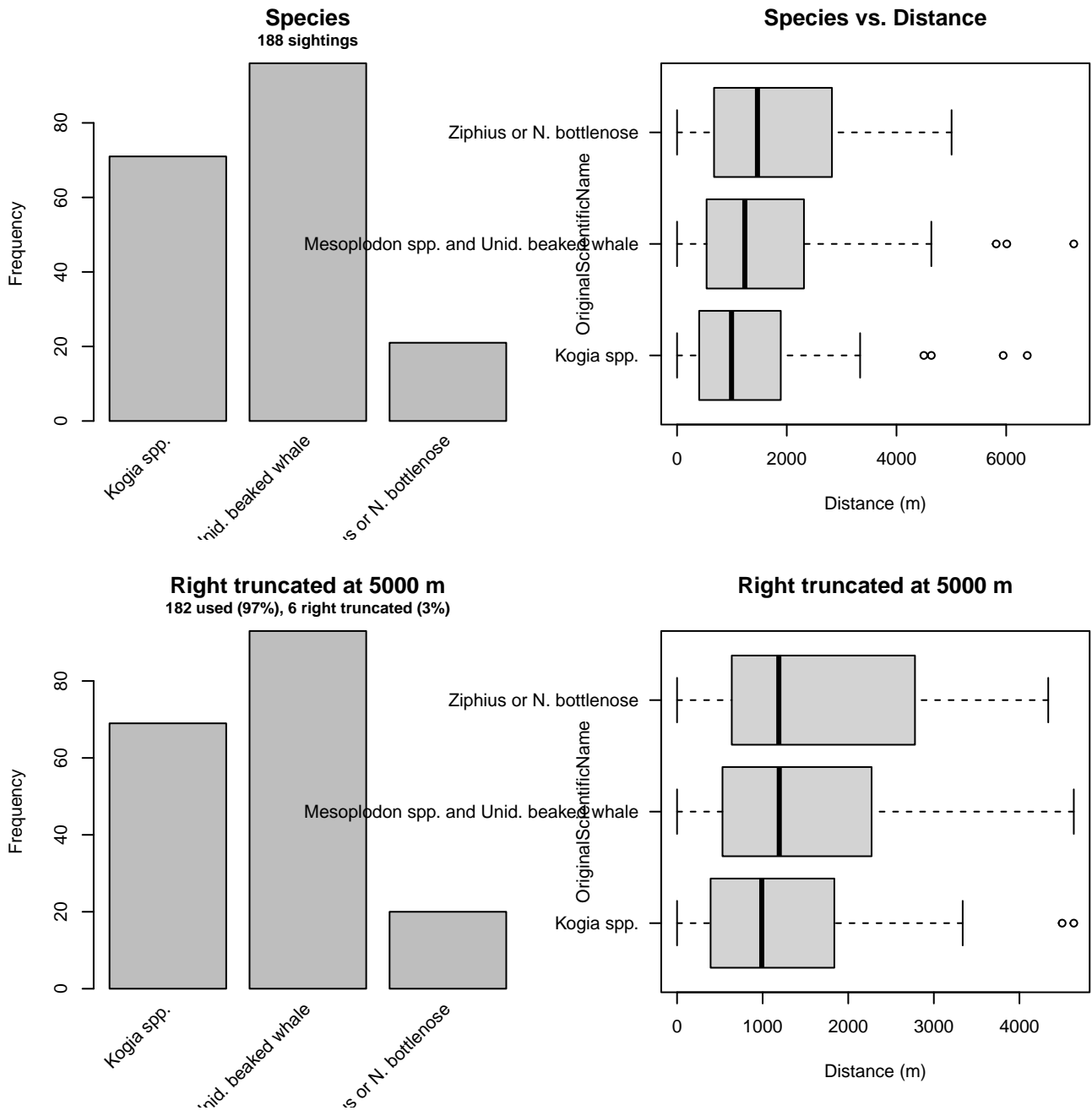


Figure 13: Distribution of the OriginalScientificName covariate before (top row) and after (bottom row) observations were truncated to fit the SEFSC detection function.

## 2.1.2 Beaked Whales

### 2.1.2.1 Shipboard Surveys

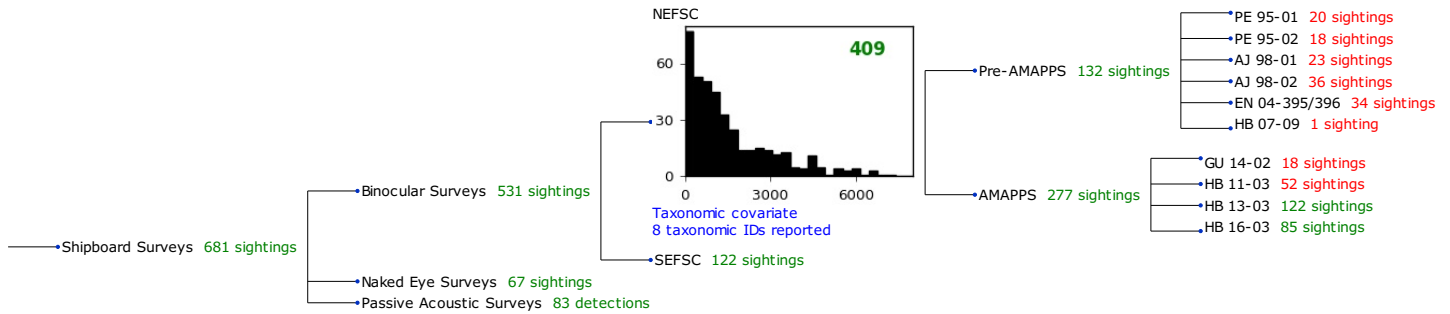


Figure 14: Detection hierarchy for shipboard surveys, showing how they were pooled during detectability modeling, for detection functions that pooled multiple taxa and used a taxonomic covariate to account for differences between them. Each histogram represents a detection function and summarizes the perpendicular distances of observations that were pooled to fit it, prior to truncation. Observation counts, also prior to truncation, are shown in green when they met the recommendation of Buckland et al. (2001) that detection functions utilize at least 60 sightings, and red otherwise. For rare taxa, it was not always possible to meet this recommendation, yielding higher statistical uncertainty. During the spatial modeling stage of the analysis, effective strip widths were computed for each survey using the closest detection function above it in the hierarchy (i.e. moving from right to left in the figure). Surveys that do not have a detection function above them in this figure were either addressed by a detection function presented in a different section of this report, or were omitted from the analysis.

#### 2.1.2.1.1 NEFSC

After right-truncating observations greater than 6000 m, we fitted the detection function to the 402 observations that remained (Table 8). The selected detection function (Figure 15) used a hazard rate key function with Beaufort (Figure 16), OriginalScientificName (Figure 17) and VesselName (Figure 18) as covariates.

Table 8: Observations used to fit the NEFSC detection function.

ScientificName	n
Hyperoodon ampullatus	4
Mesoplodon	69
Mesoplodon bidens	40
Mesoplodon densirostris	4
Mesoplodon europaeus	9
Mesoplodon mirus	7
Ziphiidae	147
Ziphius cavirostris	122
<b>Total</b>	<b>402</b>

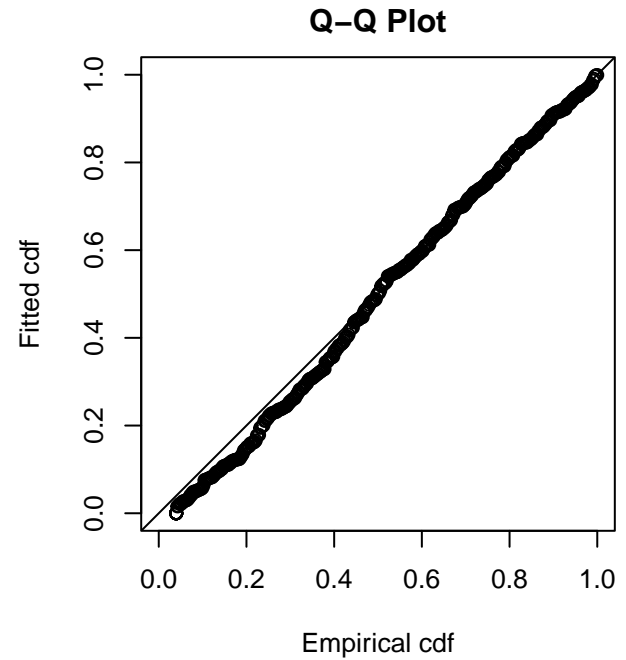
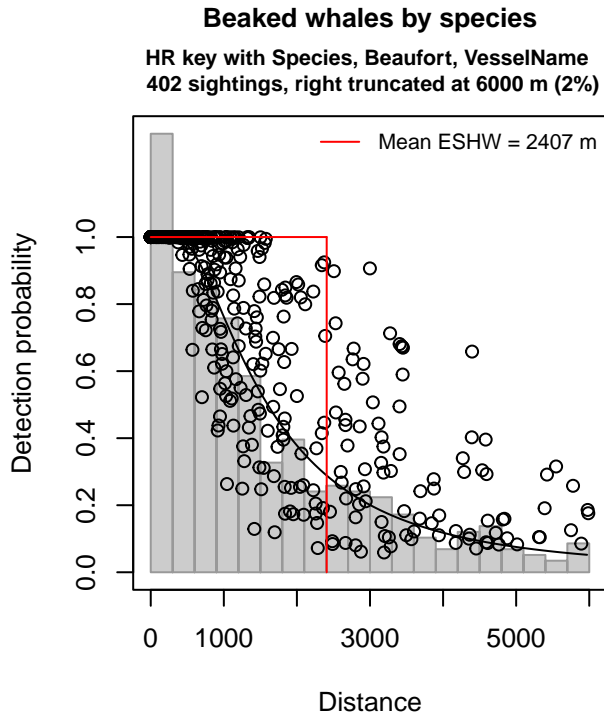


Figure 15: NEFSC detection function and Q-Q plot showing its goodness of fit.

Statistical output for this detection function:

Summary for ds object

Number of observations : 402  
 Distance range : 0 - 6000  
 AIC : 6644.8

Detection function:

Hazard-rate key function

Detection function parameters

Scale coefficient(s):

	estimate	se
(Intercept)	7.2946616	0.23066680
OriginalScientificNameN. Bottlenose or Unid. beaked whale	0.4273741	0.15634310
OriginalScientificNameZiphius cavirostris	0.2066261	0.14919980
Beaufort	-0.3259831	0.06466977
VesselNameBigelow, Endeavor, Gunter	0.7959452	0.15617439

Shape coefficient(s):

	estimate	se
(Intercept)	0.8157154	0.1116931

	Estimate	SE	CV
Average p	0.3459974	0.02233711	0.06455861
N in covered region	1161.8584040	89.48657432	0.07702021

Distance sampling Cramer-von Mises test (unweighted)

Test statistic = 0.276181 p = 0.158010

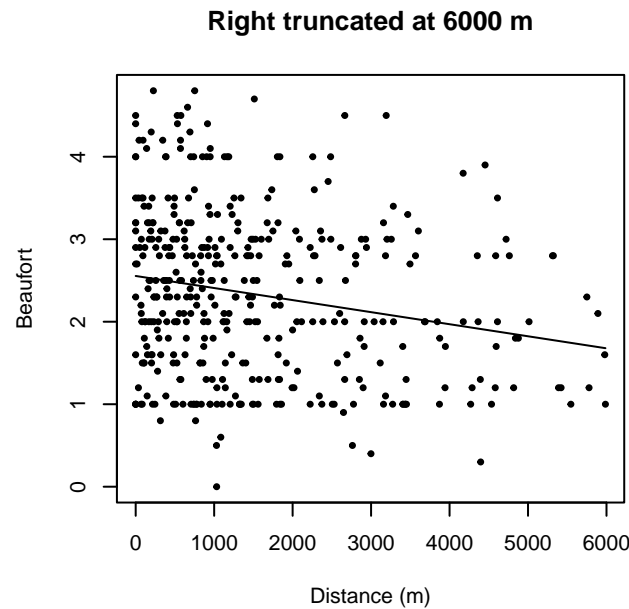
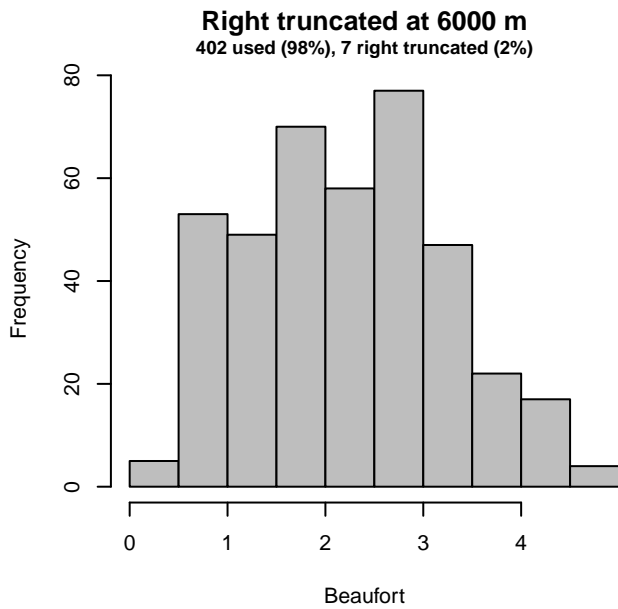
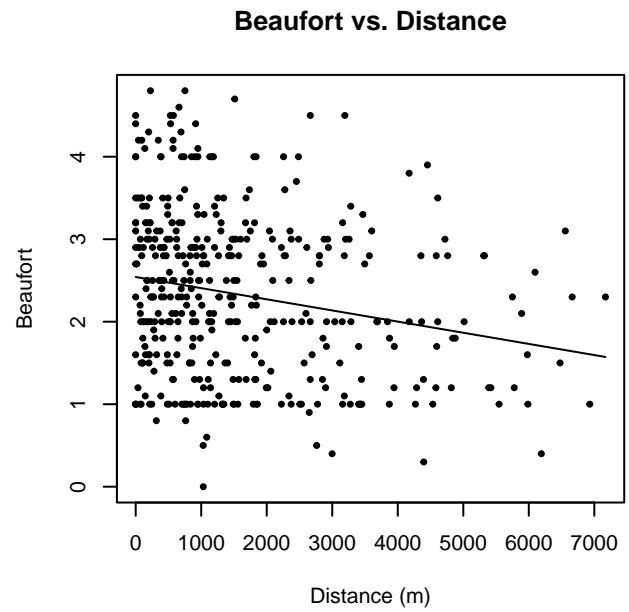
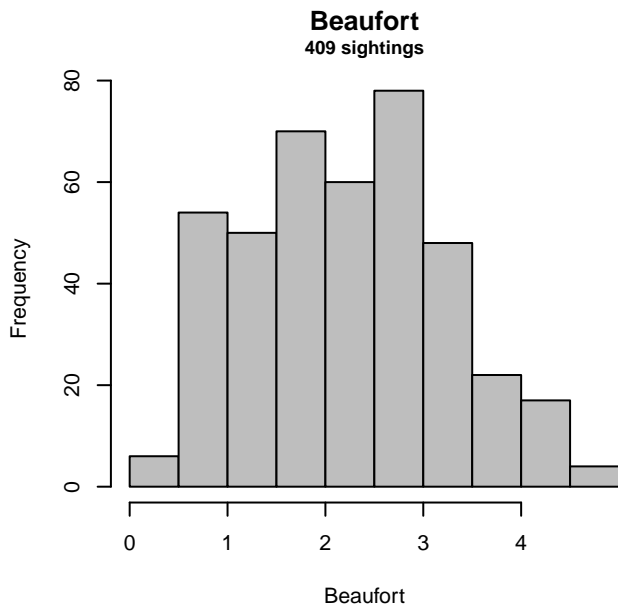


Figure 16: Distribution of the Beaufort covariate before (top row) and after (bottom row) observations were truncated to fit the NEFSC detection function.

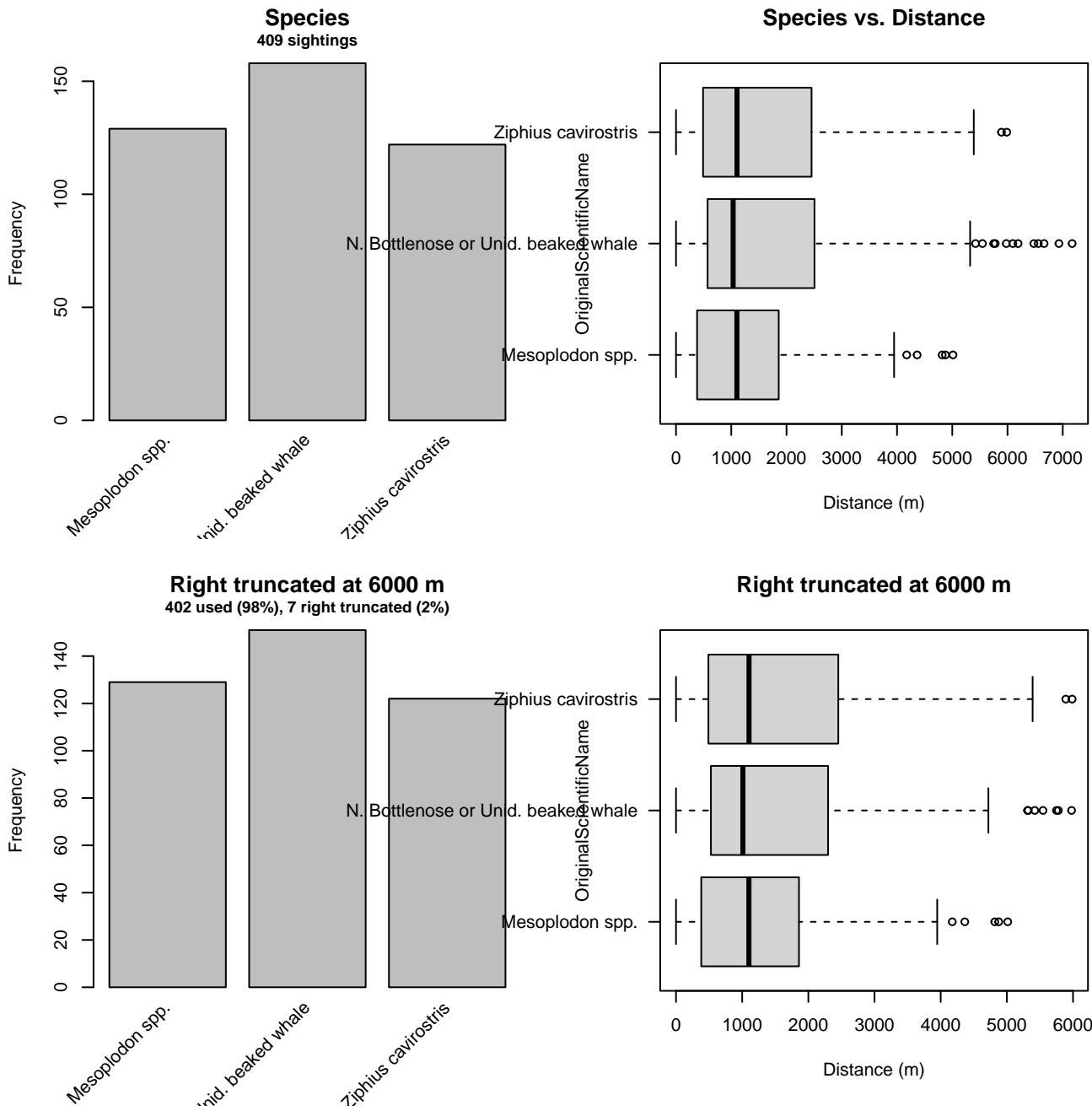


Figure 17: Distribution of the OriginalScientificName covariate before (top row) and after (bottom row) observations were truncated to fit the NEFSC detection function.

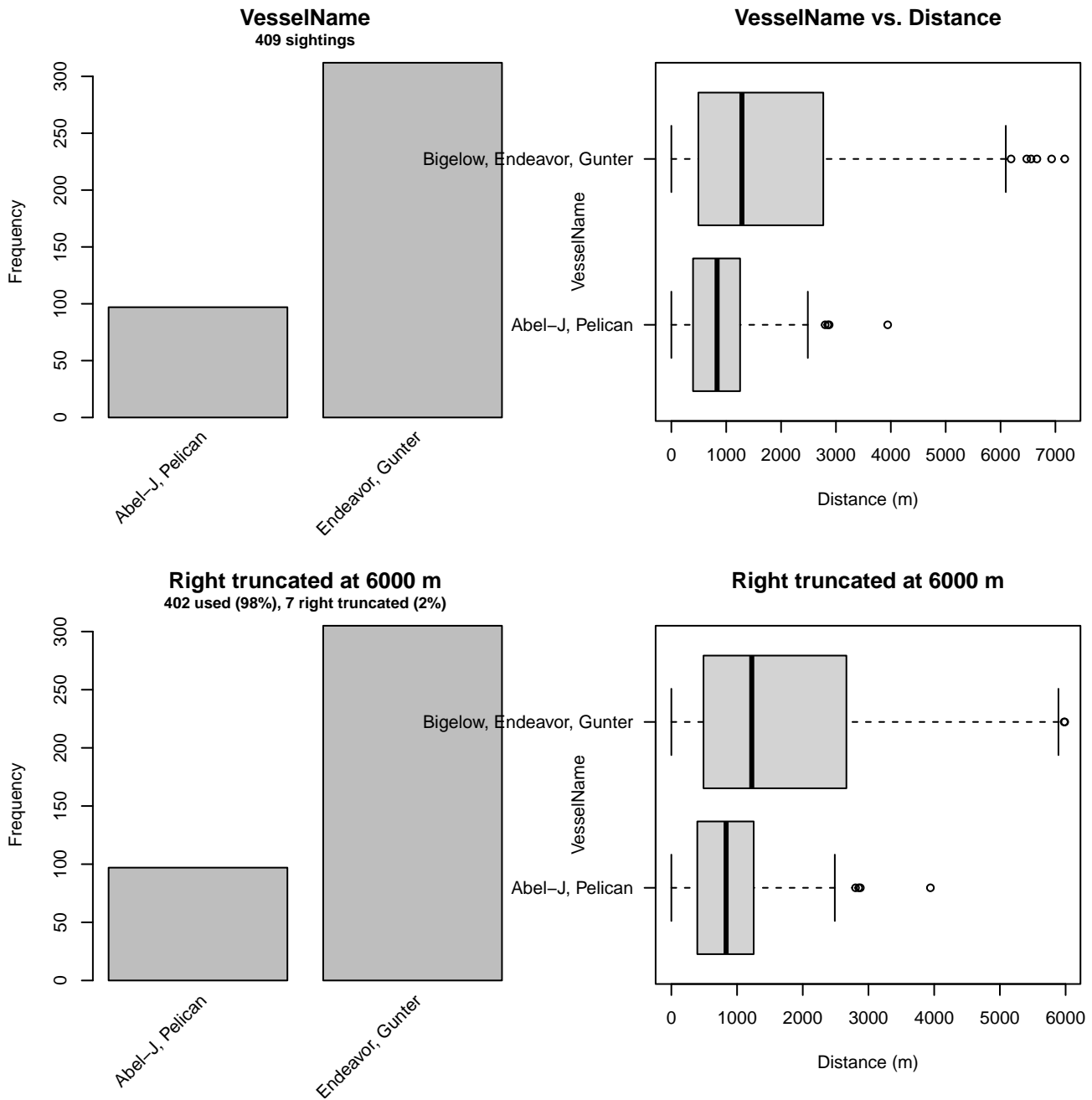


Figure 18: Distribution of the VesselName covariate before (top row) and after (bottom row) observations were truncated to fit the NEFSC detection function.

## 2.2 Without a Taxonomic Covariate

We fitted the detection functions in this section to pools of species with similar detectability characteristics but could not use a taxonomic identification as a covariate to account for differences between them. We usually took this approach after trying the taxonomic covariate and finding it had insufficient statistical power to be retained. We also resorted to it when the focal taxon being modeled had too few observations to be allocated its own taxonomic covariate level and was too poorly known for us to confidently determine which other taxa we could group it with.

## 2.2.1 Shipboard Surveys

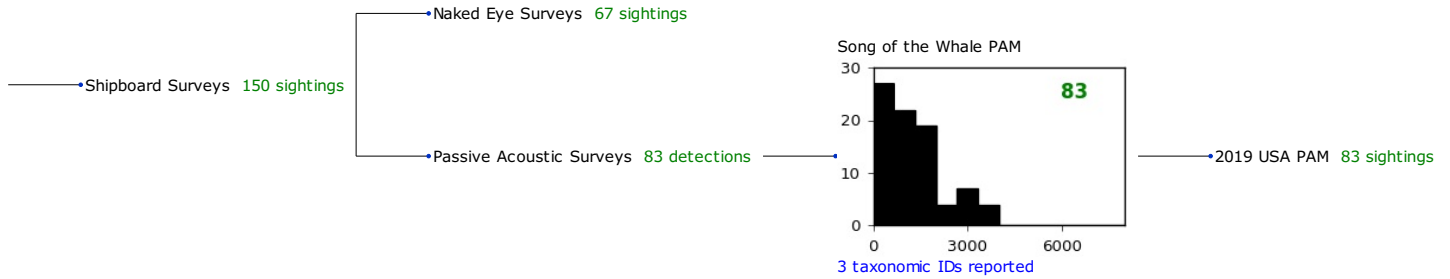


Figure 19: Detection hierarchy for shipboard surveys, showing how they were pooled during detectability modeling, for detection functions that pooled multiple taxa but could not use a taxonomic covariate to account for differences between them. Each histogram represents a detection function and summarizes the perpendicular distances of observations that were pooled to fit it, prior to truncation. Observation counts, also prior to truncation, are shown in green when they met the recommendation of Buckland et al. (2001) that detection functions utilize at least 60 sightings, and red otherwise. For rare taxa, it was not always possible to meet this recommendation, yielding higher statistical uncertainty. During the spatial modeling stage of the analysis, effective strip widths were computed for each survey using the closest detection function above it in the hierarchy (i.e. moving from right to left in the figure). Surveys that do not have a detection function above them in this figure were either addressed by a detection function presented in a different section of this report, or were omitted from the analysis.

### 2.2.1.1 Song of the Whale PAM

After right-truncating observations greater than 4000 m, we fitted the detection function to the 83 observations that remained (Table 9). The selected detection function (Figure 20) used a hazard rate key function with no covariates.

Table 9: Observations used to fit the Song of the Whale PAM detection function.

ScientificName	n
Mesoplodon bidens/densirostris	7
Mesoplodon europaeus/mirus	35
Ziphius cavirostris	41
<b>Total</b>	<b>83</b>



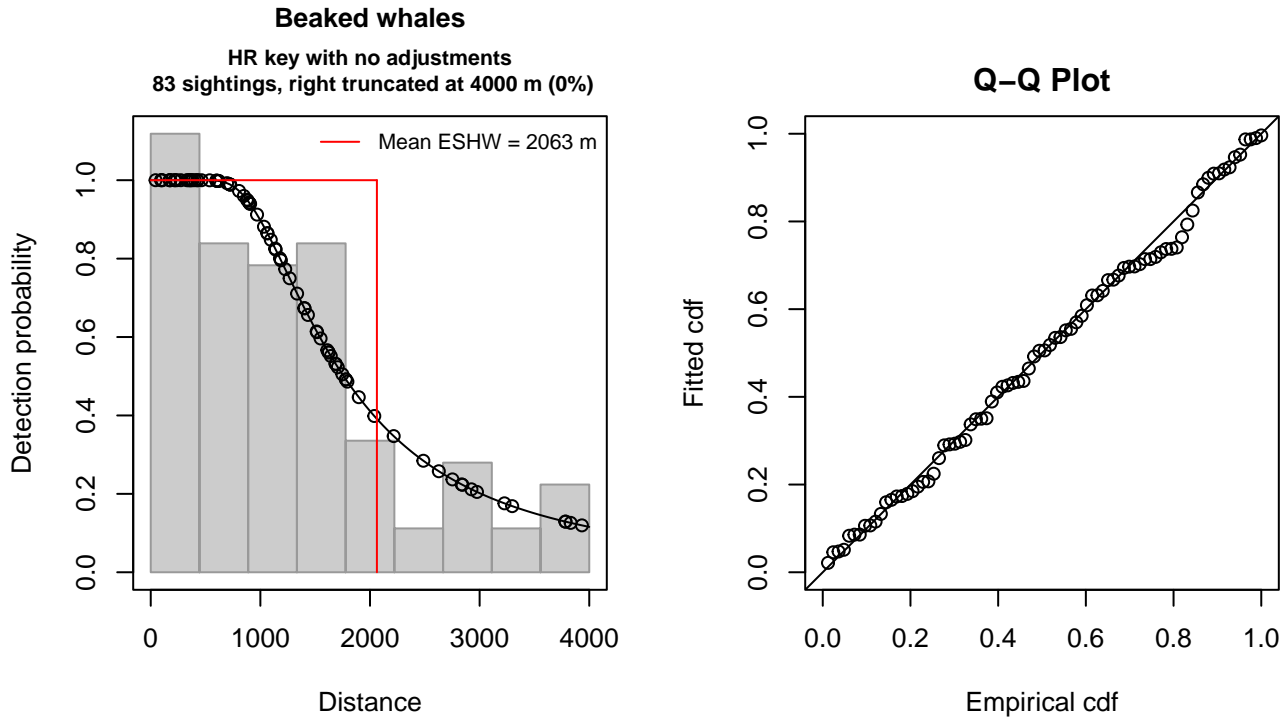


Figure 20: Song of the Whale PAM detection function and Q-Q plot showing its goodness of fit.

Statistical output for this detection function:

Summary for ds object

Number of observations : 83  
Distance range : 0 - 4000  
AIC : 1345.587

Detection function:

Hazard-rate key function

Detection function parameters

Scale coefficient(s):

	estimate	se
(Intercept)	7.299238	0.2214521

Shape coefficient(s):

	estimate	se
(Intercept)	0.7452648	0.2867125

	Estimate	SE	CV
Average p	0.5157678	0.06838478	0.1325883
N in covered region	160.9251328	24.62406127	0.1530156

Distance sampling Cramer-von Mises test (unweighted)

Test statistic = 0.030523 p = 0.974418

### 3 Bias Corrections

Density surface modeling methodology uses *distance sampling* (Buckland et al. 2001) to model the probability that an observer on a line transect survey will detect an animal given the perpendicular distance to it from the transect line. Distance sampling assumes that detection probability is 1 when perpendicular distance is 0. When this assumption is not

met, detection probability is biased high, leading to an underestimation of density and abundance. This is known as the  $g_0 < 1$  problem, where  $g_0$  refers to the detection probability at distance 0. Modelers often try to address this problem by estimating  $g_0$  empirically and dividing it into estimated density or abundance, thereby correcting those estimates to account for the animals that were presumed missed.

Two important sources of bias for visual surveys are known as *availability bias*, in which an animal was present on the transect line but impossible to detect, e.g. because it was under water, and *perception bias*, in which an animal was present and available but not noticed, e.g. because of its small size or cryptic coloration or behavior (Marsh and Sinclair 1989). Modelers often estimate the influence of these two sources of bias on detection probability independently, yielding two estimates of  $g_0$ , hereafter referred to as  $g_{0A}$  and  $g_{0P}$ , and multiply them together to obtain a final, combined estimate:  $g_0 = g_{0A} \cdot g_{0P}$ .

Our overall approach was to perform this correction on a per-observation basis, to have the flexibility to account for many factors such as platform type, surveyor institution, group size, group composition (e.g. singleton, mother-calf pair, or surface active group), and geographic location (e.g. feeding grounds vs. calving grounds). The level of complexity of the corrections varied by species according to the amount of information available, with North Atlantic right whale having the most elaborate corrections, derived from a substantial set of publications documenting its behavior, and various lesser known odontocetes having corrections based only on platform type (aerial or shipboard), derived from comparatively sparse information. Here we document the corrections used for mesoplodont beaked whales.

### 3.1 Aerial Surveys

Palka et al. (2021) developed perception bias corrections using two team, mark recapture distance sampling (MRDS) methodology (Burt et al. 2014) for aerial surveys conducted in 2010-2017 by NOAA NEFSC and SEFSC during the AMAPPS program. These were the only extant perception bias estimates developed from aerial surveys used in our analysis, aside from estimates developed earlier by Palka and colleagues (Palka 2006; Palka et al. 2017). Those earlier efforts utilized older methods and less data than their 2021 analysis, so we applied the Palka et al. (2021) estimates to all aerial survey programs (Table 10).

We applied Palka’s estimate for NEFSC to all programs other than SEFSC on the basis that those programs employed a similar visual scanning protocol that allowed observers to scan from the trackline up to the horizon, while SEFSC’s protocol generally limited scanning only up to  $50^\circ$  from the trackline, resulting in a smaller effective strip width.

We caution that it is possible that perception bias was different on the other aerial programs, as they often used different aircraft, flew at different altitudes, and were staffed by different personnel. Of particular concern are that many programs flew Cessna 337 Skymasters, which had flat windows, while NOAA flew de Havilland Twin Otters, which had bubble windows, which likely afforded a better view of the transect line and therefore might have required less of a correction than the Skymasters. Correcting the other programs using NOAA’s estimate as we have done is likely to yield less bias than leaving them uncorrected, but we urge all programs to undertake their own efforts to estimate perception bias, as resources allow.

We estimated availability bias corrections using the Laake et al. (1997) estimator and dive intervals reported by Palka et al. (2017) (Table 11). To estimate time in view, needed by the Laake estimator, we used results reported by Robertson et al. (2015), rescaled linearly for each survey program according to its target altitude and speed. We computed availability bias corrections for a single individual of the three Mesoplodont species for which we have dive data. These included Sowerby’s (Palka et al. 2021), True’s (Engelhaupt pers. comm.) and Blainville’s beaked whales (Tyack et al. 2006). We then averaged the availability corrections. We believed this to be an adequate way to represent Mesoplodont beaked whales in our analysis, but recommend a more sophisticated approach like a Monte Carlo simulation in future efforts.

We caution that Robertson’s analysis was done for a de Havilland Twin Otter, which may have a different field of view than that of the other aircraft used here, which mainly comprised Cessna 337 Skymasters with flat windows but also a Partenavia P-68 with bubble windows (on the NYS-DEC/TT surveys). However, we note that McLellan et al. (2018) conducted a sensitivity analysis on the influence of the length of the “window of opportunity” to view beaked whales from a Cessna Skymaster on their final density estimates and found that they varied by only a few thousandths of an animal per kilometer when the window of opportunity more than doubled. Still, we urge additional program-specific research into estimation of availability bias.

To address the influence of group size on availability bias, we applied the group availability estimator of McLellan et al. (2018) on a per-observation basis. Following Palka et al. (2021), who also used that method, we assumed that individuals in the group dived asynchronously. The resulting  $g_{0A}$  corrections ranged from about 0.15 to 0.65 (Figure 21). We caution that the assumption of asynchronous diving can lead to an underestimation of density and abundance if diving is actually synchronous; see McLellan et al. (2018) for an exploration of this effect. However, if future research finds that this species conducts synchronous dives and characterizes the degree of synchronicity, the model can be updated to account for this knowledge.

Table 10: Perception bias corrections for mesoplodont beaked whales applied to aerial surveys.

Surveys	Group Size	$g_{0P}$	$g_{0P}$ Source
SEFSC	Any	0.86	Palka et al. (2021): SEFSC
All others	Any	0.62	Palka et al. (2021): NEFSC

Table 11: Surface and dive intervals for mesoplodont beaked whales used to estimate availability bias corrections.

Species	Surface Interval (s)	Dive Interval (s)	Source
True’s beaked whale	177	813.0	Palka et al. (2021)
Sowerby’s beaked whale	360	1242.0	Engelhaupt (2022, pers.comm.)
Blainville’s beaked whale	228	1685.2	Tyack et al. (2006)

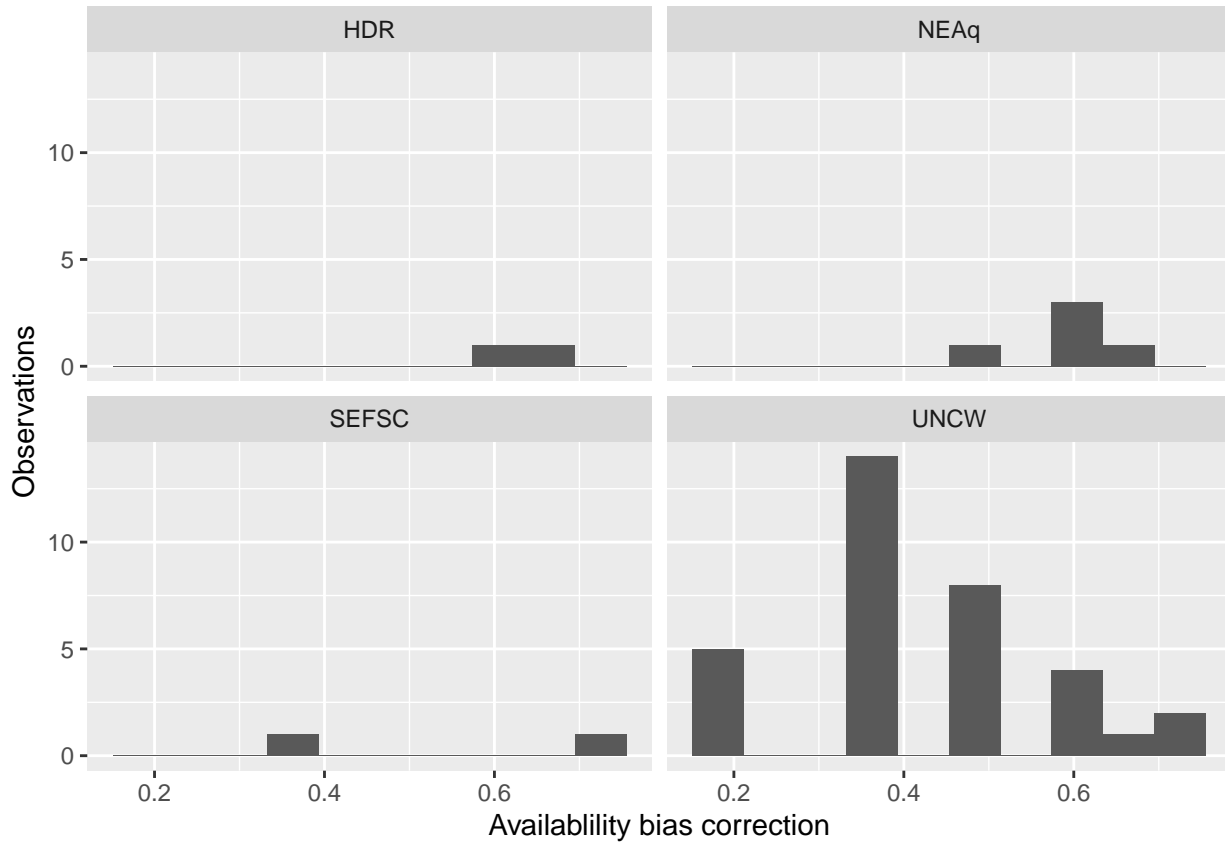


Figure 21: Availability bias corrections for mesoplodont beaked whales for aerial surveys, by institution.

### 3.2 Shipboard Surveys

Most of the shipboard surveys in our analysis used high-power (25x150), pedestal-mounted binoculars. Similar to aerial surveys, Palka et al. (2021) developed perception bias corrections using two team, MRDS methodology (Burt et al. 2014) for high-power binocular surveys conducted in 2010-2017 by NOAA NEFSC and SEFSC during the AMAPPS program. These were the only extant perception bias estimates developed from high-power binocular surveys used in our analysis, aside from estimates developed earlier by Palka and colleagues (Palka 2006; Palka et al. 2017). Those earlier efforts utilized older methods and less data than their 2021 analysis, so we applied the Palka et al. (2021) estimates for perception bias to all shipboard surveys that searched with high-power binoculars (Table 12).

We applied Barlow (1999) availability bias estimates for Mesoplodont species to shipboard NEFSC and SEFCS high-power binocular surveys.

There were no naked eye surveys for Mesoplodont beaked whales used in this analysis. However, we did use data from

MCR’s Song of the Whale 2019 MAPS passive acoustic monitoring (PAM) survey. For this survey, we applied an availability correction that accounts for proportion of time that beaked whales click during their dive cycles. Following Barlow et al. 2013,  $g(0)$  for availability was estimated as 0.43 (CV 0.03):  $g(0) = (E(a) + t) / (E(a) + E(u))$  Where  $E(a)$  is the expected time for which a whale is available for detection (i.e. foraging time), and  $t$  is the time window during which an animal could feasibly be detected, which is twice the effective strip width divided by the average survey speed, and  $E(u)$  is the expected time for which a whale is unavailable for detection, which is the time between foraging events. As whales can theoretically be detected both ahead of and behind the array up to a distance equal to the effective strip half width (EShW) estimated when modelling the detection function, the time window  $t$  can be defined as twice the EShW divided by average survey speed. The variance for  $g(0)$  over a finite time window was estimated using the delta method (Seber et al. 1982). As the estimates made by Barlow et al. (2013) for Cuvier’s beaked whales used data from a variety of non-Atlantic locations (Ligurian Sea, Hawaii and Southern California), supplementary dive data were incorporated from satellite tags deployed off North Carolina between 2014 and 2016 (Shearer et al. 2019).

We assumed perception bias on this survey was equal to 1.

Table 12: Perception and availability bias corrections for mesoplodont beaked whales applied to shipboard surveys.

Surveys	Searching Method	Group Size	$g_{0P}$	$g_{0P}$ Source	$g_{0A}$	$g_{0A}$ Source
NEFSC	Binoculars	Any	0.42	Palka et al. (2021): NEFSC	0.98	Barlow (1999)
SEFSC	Binoculars	Any	0.32	Palka et al. (2021): SEFSC	0.98	Barlow (1999)
MCR	Acoustic	Any	1.00	Assumed	0.43	Boisseau et al. (in review)

## 4 Density Model

There are four species of the genus *Mesoplodon* that occur in the western North Atlantic. These include True’s beaked whale, *M. mirus*; Gervais’ beaked whale, *M. europaeus*; Blainville’s beaked whale, *M. densirostris*; and Sowerby’s beaked whale, *M. bidens* (Mead 1989). In addition to these four species, unidentified Mesoplodont sightings were also included in this species guild for modeling purposes. Their cryptic surface behavior makes it difficult to visually identify Mesoplodont to the species level at sea, however these species are acoustically identifiable. As shown in Table 13, there were few observations identified to the species level available for use in this study. As such Mesoplodont species were modeled as a guild.

Table 13: Mesoplodont Observations by Species

ScientificName	n
<i>Mesoplodon</i>	118
<i>Mesoplodon bidens</i>	31
<i>Mesoplodon bidens/densirostris</i>	6
<i>Mesoplodon densirostris</i>	2
<i>Mesoplodon europaeus</i>	17
<i>Mesoplodon europaeus/mirus</i>	12
<i>Mesoplodon mirus</i>	8

Off the U.S. Atlantic coast, Mesoplodont beaked whale observations have primarily occurred along the shelf-edge and in deep waters (Tove 1995; Hamazaki 2002; Palka 2006; Hayes et al. 2020). The survey segments with observations used in this study occurred between 99 m to 5096 m depth, with only 16 observations occurring in waters shallower than 900 m. The sea surface salinity of segments with observations ranged from 32 to 36. Similar to Cuvier’s beaked whales these species feed on squid and benthic fish, are deep diving, occur in small groups, are cryptic at the surface and are vocally active during foraging dives. It is probable that like Cuvier’s beaked whales their habitat preferences include deep waters with depths greater than 1,000 m (Baird et al. 2004) and static bathymetric features such as canyons, seamounts and shelf-edges (Waring et al. 2001; MacLeod et al. 2005; Moulins et al. 2007). These features likely help concentrate prey and thus provide ideal foraging habitat (Baumgartner 1997; Moulins et al. 2007).

It should be noted that the four species of Mesoplodonts likely have different habitat requirements and preferences, and niche partitioning has been proposed for north Atlantic beaked whale species (MacLeod and Zuur 2005). As such, a guild model may overly simplify habitat relationships for these species. True’s beaked whales are considered a temperate species and has been sighted between Nova Scotia and the Bahamas (Mead 1989; Macleod et al. 2006; Hayes et al. 2020). Gervais’ beaked

whales are considered largely an oceanic species and strandings have been reported from Cape Cod to Florida in the western North Atlantic (Mead 1989; Macleod et al. 2006; McLellan et al. 2018; Hayes et al. 2020). Blainville's beaked whales have been reported from southwestern Nova Scotia to Florida and are considered widely distributed in the Atlantic (Mead 1989; Macleod et al. 2006; McLellan et al. 2018; Hayes et al. 2020). Sowerby's beaked whales have the most northerly distribution of the Mesoplodont species and have been observed from New England up to the ice pack in the Davis Strait (Mead 1989; Macleod et al. 2006; Jefferson et al. 2008; Hayes et al. 2020).

Stanistreet et al. (2017) described the presence of beaked whales from six passive acoustic monitoring sites in the western North Atlantic along the continental shelf between the Gully in the north and Jacksonville in the south between 2011 and 2015. The authors observed considerable variation in relative species occurrence across the study region. Sowerby's beaked whales were most prevalent at the mid gully recorder and not south of Hatteras, Gervais beaked whale was present from George's bank to Jacksonville with the highest number of detections occurring at Onslow Bay and Blainville's beaked whales were detected from Hatteras to Jacksonville. It is important to note here that True's beaked whale had not yet been acoustically identified and so there may be some Gervais detections that actually represent True's beaked whale (Stanistreet et al. 2017).

Cohen et al. (2022) detected Mesoplodont clicks at 11 acoustic monitoring sites from Heezen Canyno in the north to Jacksonville in the south between 2016 and 2019. In this study Blainville's beaked whale was found to be most prevalent at Blake Spur and showed a slight decline in summer. Presence was negligible at other sites but a slight spring increase in detection was evident at the Gulf Stream and Blake Plateau sites (Cohen et al. 2022). Sowerby's beaked whale acoustic presence was reportedly low at all sites, but a maxima in presence was seen at Wilmington and Heezen Canyons with highest presence reported in spring and the lowest in fall (Cohen et al. 2022). Gervais' beaked whale was found to have a strictly southerly distribution with the highest number of detections at the Gulf Stream and Blake Plateau sites and in lower levels at Hatteras and Blake Spur and absent from Jacksonville (Cohen et al. 2022). The authors reported a distinct seasonal pattern not reported by previous studies and identified an increase in presence at the Gulf Stream and Blake Plateau sites in fall with a maximum in winter. Finally, True's beaked whales were identified in this study and detected at very low levels at all monitoring sites north of Hatteras. A clear seasonal pattern was visible, with increased presence in both the summer and the winter compared to the fall and the spring, and lowest overall presence was identified in the fall. Highest acoustic presence was seen at Norfolk Canyon in all seasons except fall (Cohen et al. 2022).

Given that Mesoplodont species were reported year-round with no known seasonal trend that held true for all species within the guild, we chose to fit year-round models to the entire study area, and as with Cuvier's beaked whales we chose to model from 2010 through 2019, which eliminated 35 sightings. Again, we eliminated 2020 from the models so that we could use micronekton biomass, distance to eddies and kinetic energy covariates as candidates in the model.

The Mesoplodont model contained over 769,000 km of segments with 194 total observations. The top model, selected with the highest explained deviance and lowest AIC and REML scores, was a contemporaneous model. A total of seven covariates were retained in the top model, including an interaction term of Depth:Slope, biomass of mesopelagic micronekton, sea surface salinity (SSS), total kinetic energy (TKE), distance to eddies, distance to seamounts and distance to the 1500 m isobath (Table 14) (Figure 25). The relationship to the bivariate term Depth:Slope indicated more animals in deep waters with high slope. There was a positive relationship to lower mesopelagic micronekton with abundance increasing as lower mesopelagic biomass increased. There was a largely negative relationship to sea surface salinity, whereby more animals were predicted in northern waters, which are fresher, and lower density was predicted on the Blake Plateau and offshore of it by the Blake Spur, where waters are saltier. There was a positive relationship to total kinetic energy, which showed more animals at higher values of TKE. In the East Coast study area, places of highest total kinetic energy are in the Gulf Stream. TKE is a relatively stable covariate probably used by the model to capture high density along the slope just south of Cape Hatteras, where the Gulf Stream departs the continental shelf, and offshore near the north wall of the Gulf Stream. The relationship to distance to eddies showed a peak in densities between 50 and 250 km from eddies. There was a negative relationship to distance to seamounts, which indicated that Mesoplodont species abundance increased near seamounts. This is consistent with known beaked whale relationships to static bathymetric features, which may help to concentrate prey and therefore provide good foraging habitat (Baumgartner 1997; Moulins et al. 2007). And finally, there was a positive relationship to distance to the 1500 m isobath. This covariate was likely used by the model to capture higher abundance in offshore regions for these species.

## 4.1 Final Model

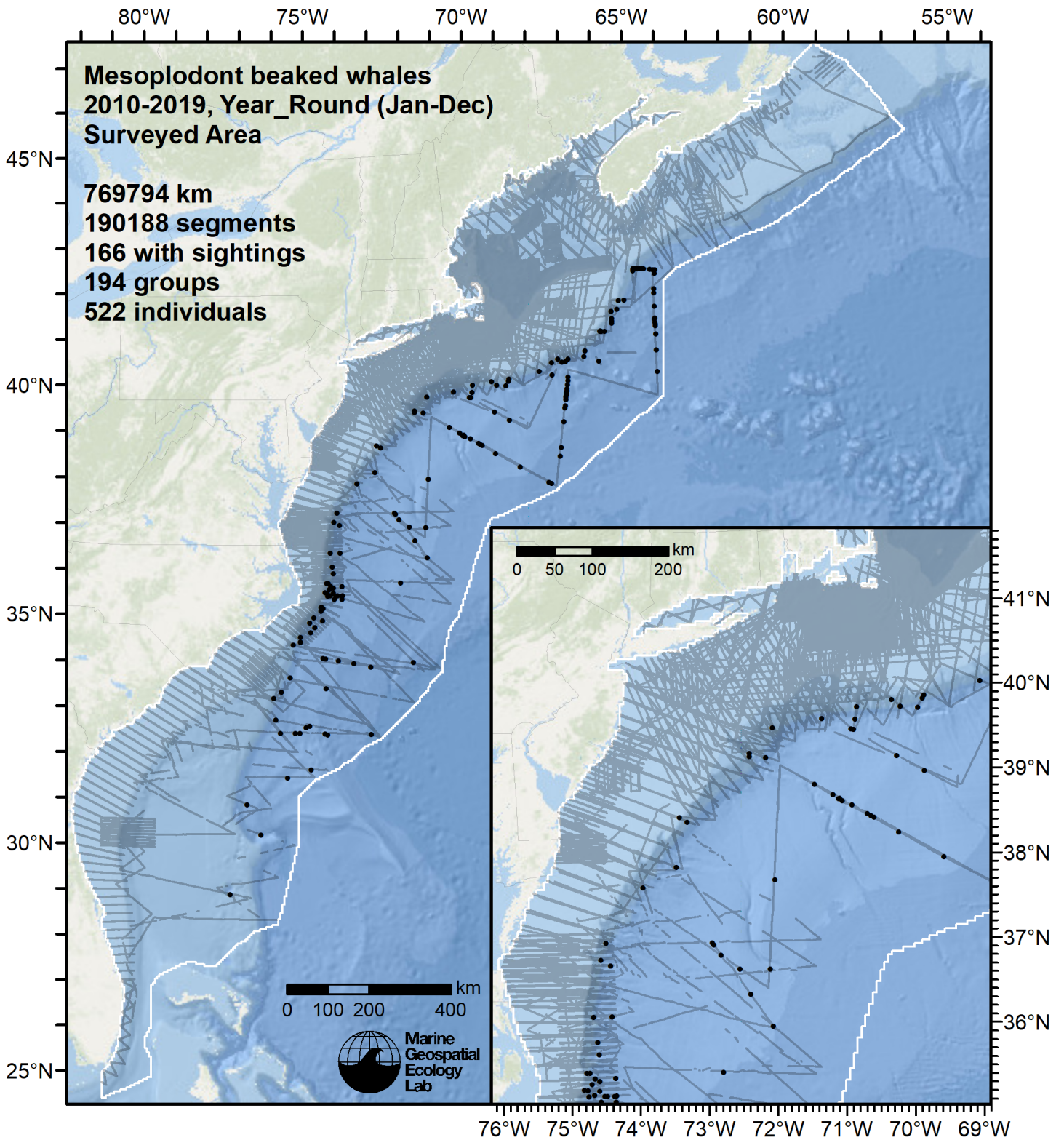


Figure 22: Survey segments used to fit the model. Black points indicate segments with observations.

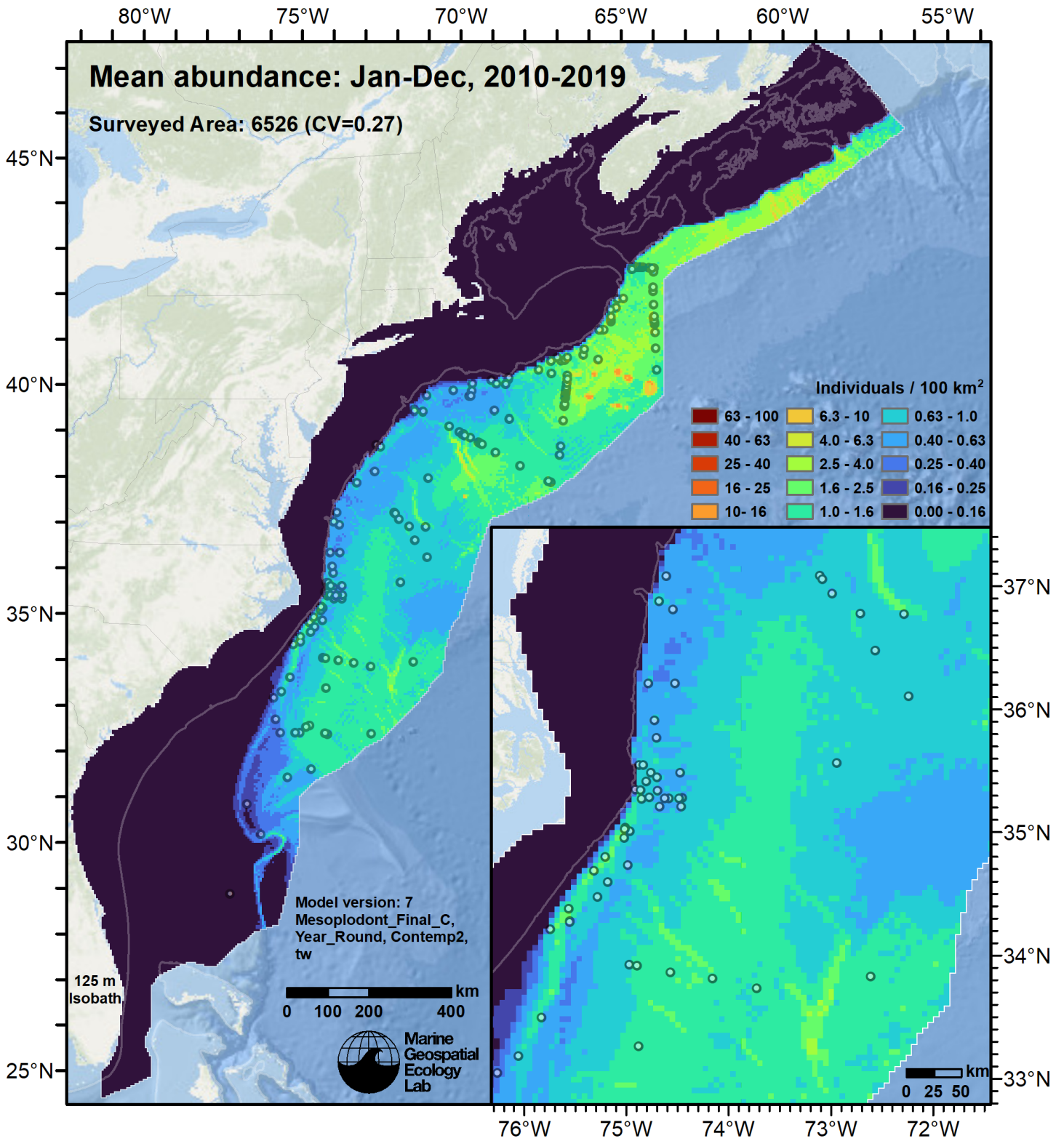


Figure 23: Mesoplodont beaked whales mean density for the indicated period, as predicted by the model. Open circles indicate segments with observations. Mean total abundance and its coefficient of variation (CV) are given in the subtitle. Variance was estimated with the analytic approach given by Miller et al. (2022), Appendix S1, and accounts both for uncertainty in model parameter estimates and for seasonal and interannual variability in dynamic covariates.

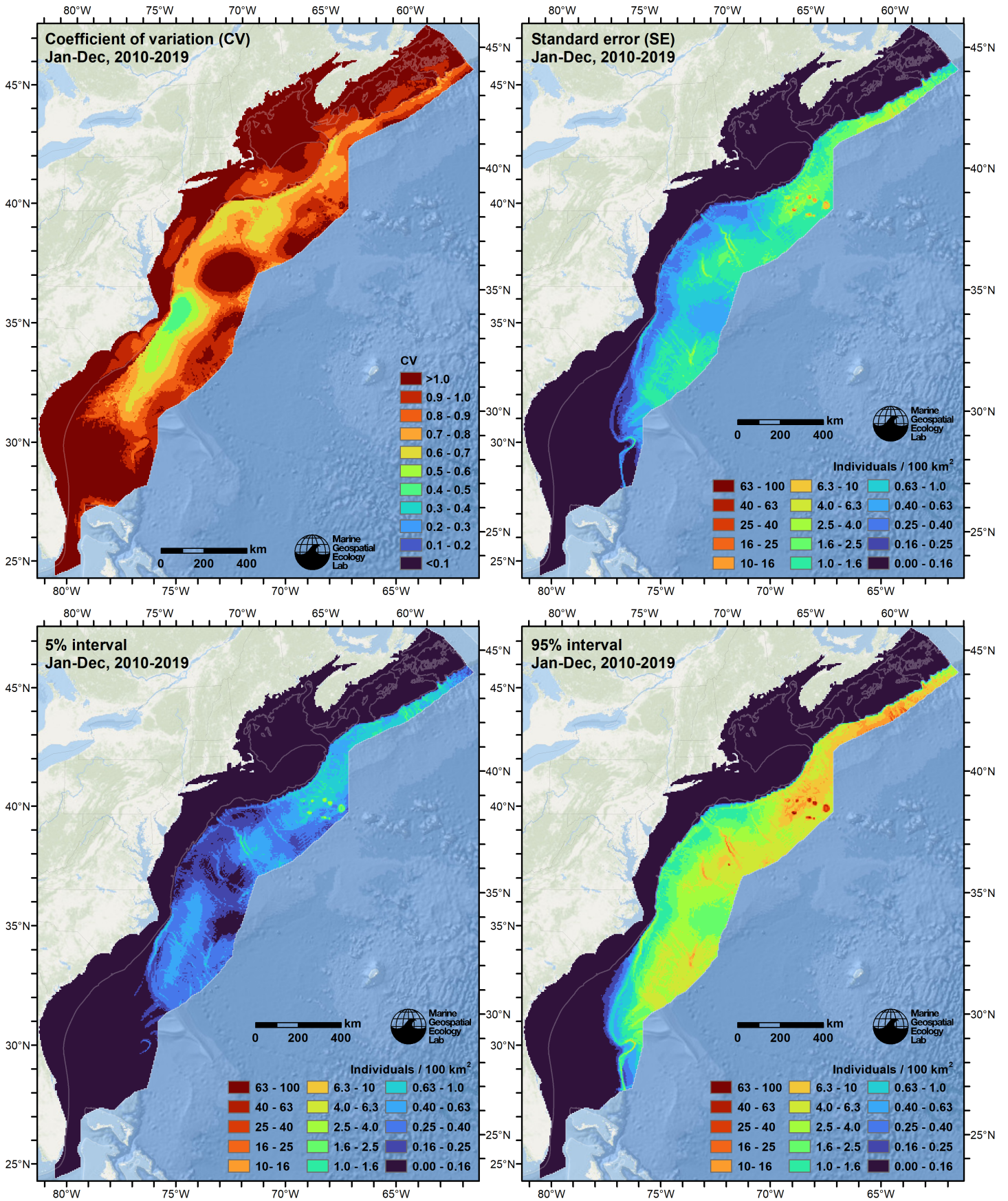


Figure 24: Uncertainty statistics for the mesoplodont beaked whales mean density surface (Figure 23) predicted by the model. Variance was estimated with the analytic approach given by Miller et al. (2022), Appendix S1, and accounts both for uncertainty in model parameter estimates and for seasonal and interannual variability in dynamic covariates.



Statistical output for this model:

Family: Tweedie(p=1.195)

Link function: log

Formula:

```
IndividualsCorrected ~ offset(log(SegmentArea)) + te(log10(pmax(10,
  Depth)), log10((pmax(0.3, pmin(Slope, 30))))), bs = "ts") +
  s(log10(pmax(0.01, pmin(MnkLMeso, 5))), bs = "ts") + s(pmax(31,
  SSS_HYCOM), bs = "ts") + s(log10(pmax(0.002, TKE)), bs = "ts") +
  s(pmin(I(DistToEddy/1000), 350), bs = "ts") + s(pmin(I(DistToSmt/1000),
  800), bs = "ts") + s(pmax(-300, pmin(I(DistTo1500m/1000),
  100)), bs = "ts")
```

Parametric coefficients:

```
      Estimate Std. Error t value Pr(>|t|)
(Intercept) -25.8997      0.6656  -38.91  <2e-16 ***
```

---

Signif. codes: 0 '\*\*\*' 0.001 '\*\*' 0.01 '\*' 0.05 '.' 0.1 ' ' 1

Approximate significance of smooth terms:

	edf	Ref.df
te(log10(pmax(10, Depth)),log10((pmax(0.3, pmin(Slope, 30)))))	2.9429	24
s(log10(pmax(0.01, pmin(MnkLMeso, 5))))	1.0025	9
s(pmax(31, SSS_HYCOM))	2.2760	9
s(log10(pmax(0.002, TKE)))	0.8502	9
s(pmin(I(DistToEddy/1000), 350))	3.6812	9
s(pmin(I(DistToSmt/1000), 800))	0.9391	9
s(pmax(-300, pmin(I(DistTo1500m/1000), 100)))	1.1107	9
	F	p-value
te(log10(pmax(10, Depth)),log10((pmax(0.3, pmin(Slope, 30)))))	0.827	2.37e-05
s(log10(pmax(0.01, pmin(MnkLMeso, 5))))	1.608	4.66e-06
s(pmax(31, SSS_HYCOM))	1.939	4.72e-05
s(log10(pmax(0.002, TKE)))	0.524	0.015246
s(pmin(I(DistToEddy/1000), 350))	4.206	< 2e-16
s(pmin(I(DistToSmt/1000), 800))	1.124	0.000631
s(pmax(-300, pmin(I(DistTo1500m/1000), 100)))	1.395	0.000121

```
te(log10(pmax(10, Depth)),log10((pmax(0.3, pmin(Slope, 30)))) ***
s(log10(pmax(0.01, pmin(MnkLMeso, 5)))) ***
s(pmax(31, SSS_HYCOM)) ***
s(log10(pmax(0.002, TKE))) *
s(pmin(I(DistToEddy/1000), 350)) ***
s(pmin(I(DistToSmt/1000), 800)) ***
s(pmax(-300, pmin(I(DistTo1500m/1000), 100))) ***
```

---

Signif. codes: 0 '\*\*\*' 0.001 '\*\*' 0.01 '\*' 0.05 '.' 0.1 ' ' 1

R-sq.(adj) = 0.0323 Deviance explained = 46.7%

-REML = 1366.7 Scale est. = 15.387 n = 190188

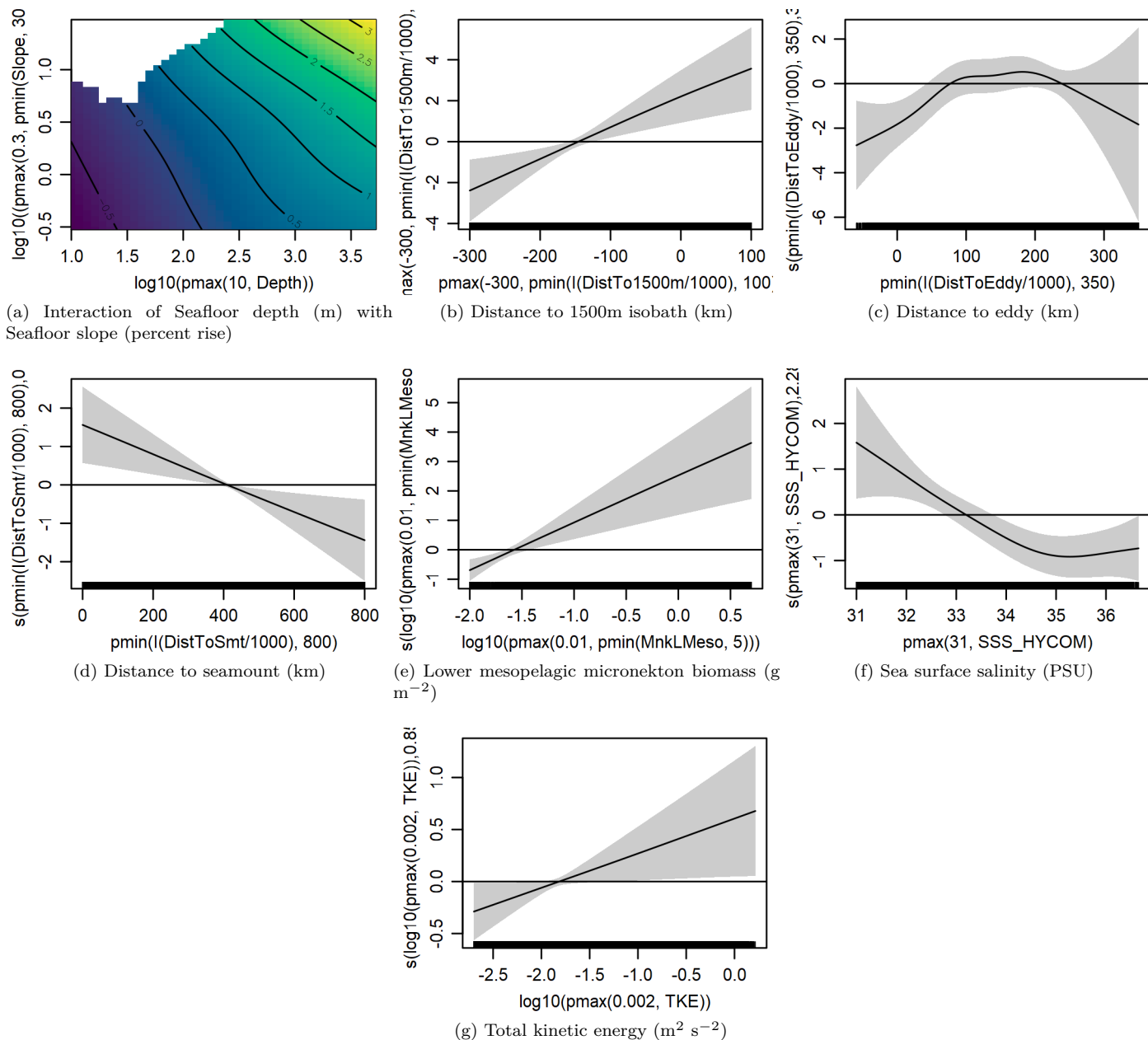


Figure 25: Functional plots for the final model. Transforms and other treatments are indicated in axis labels.  $\log_{10}$  indicates the covariate was  $\log_{10}$  transformed.  $pmax$  and  $pmin$  indicate the covariate's minimum and maximum values, respectively, were Winsorized to the values shown. Winsorization was used to prevent runaway extrapolations during prediction when covariates exceeded sampled ranges, or for ecological reasons, depending on the covariate.  $/1000$  indicates meters were transformed to kilometers for interpretation convenience.

Table 14: Covariates used in the final model.

Covariate	Description
Depth	Depth (m) of the seafloor, from SRTM30_PLUS (Becker et al. (2009))
DistTo1500m	Distance (km) to the 1500m isobath, derived from SRTM30_PLUS (Becker et al. (2009))
DistToEddy	Monthly mean distance (km) to the edge of the closest mesoscale eddy of any polarity and age, derived with MGET (Roberts et al. (2010)) from the Aviso Mesoscale Eddy Trajectories Atlas (META2.0), produced by SSALTO/DUACS and distributed by AVISO+ ( <a href="https://aviso.altimetry.fr">https://aviso.altimetry.fr</a> ) with support from CNES, in collaboration with Oregon State University with support from NASA, using the method of Schlax and Chelton (2016), based on Chelton et al. (2011)

Table 14: Covariates used in the final model. (continued)

Covariate	Description
DistToSmt	Distance (km) to the closest seamount, derived from the Harris et al. (2014) geomorphology
MnkLMeso	Monthly mean micronekton biomass available in the lower mesopelagic zone, expressed as wet weight ( $\text{g m}^{-2}$ ), from SEAPODYM (Lehodey et al. (2008); Lehodey et al. (2015)), provided by E.U. Copernicus Marine Service. doi: <a href="https://doi.org/10.48670/moi-00020">10.48670/moi-00020</a> . Computed as the sum of the SEAPODYM mnkc_lmeso, mnkc_mlmeso, and mnkc_hmlmeso variables.
SSS_HYCOM	Monthly mean sea surface salinity (PSU) from the HYCOM GOFS 3.1 $1/12^\circ$ ocean model (Chassignet et al. (2009))
Slope	Slope (percent rise) of the seafloor, derived from SRTM30_PLUS (Becker et al. (2009))
TKE	Monthly mean total kinetic energy ( $\text{m}^2 \text{s}^{-2}$ ) derived from Aviso Ssalto/Duacs global gridded L4 reprocessed geostrophic currents, produced and distributed by E.U. Copernicus Marine Service. doi: <a href="https://doi.org/10.48670/moi-00148">10.48670/moi-00148</a>

## 4.2 Diagnostic Plots

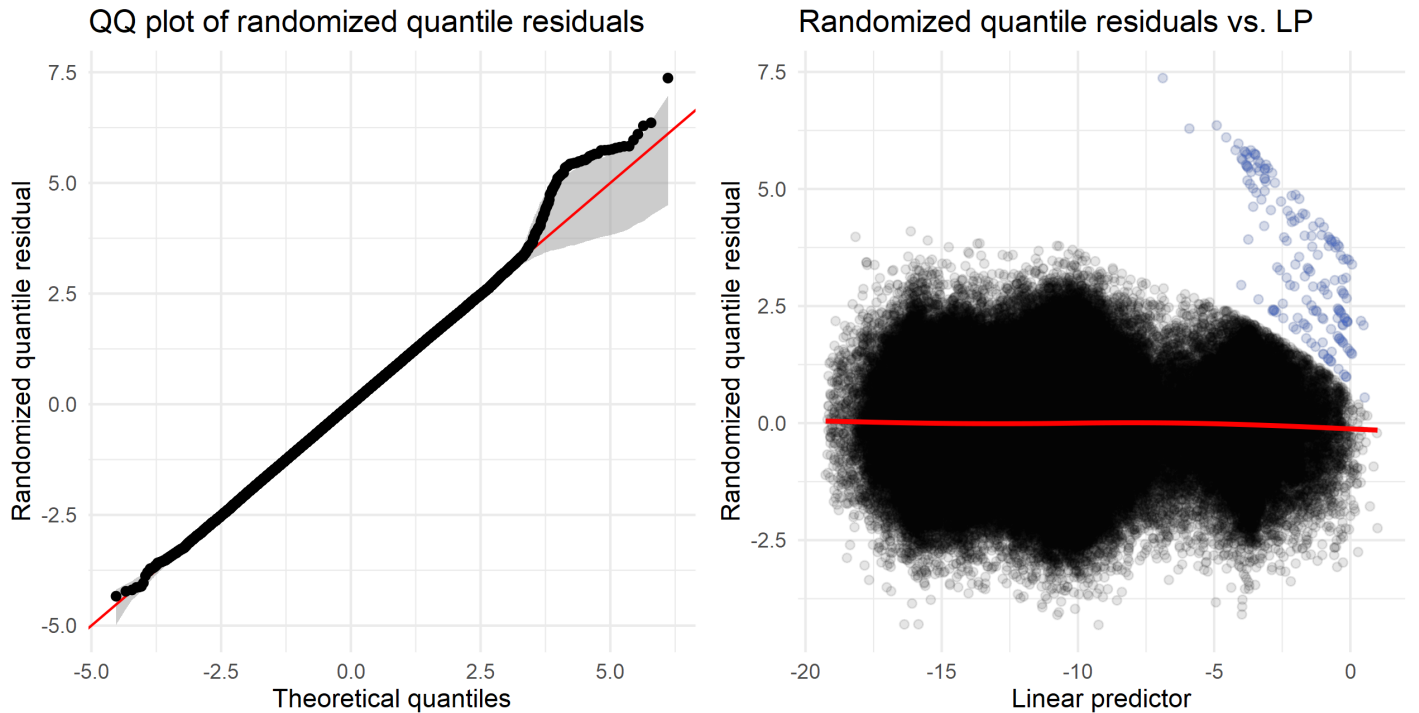


Figure 26: Residual plots for the final model.

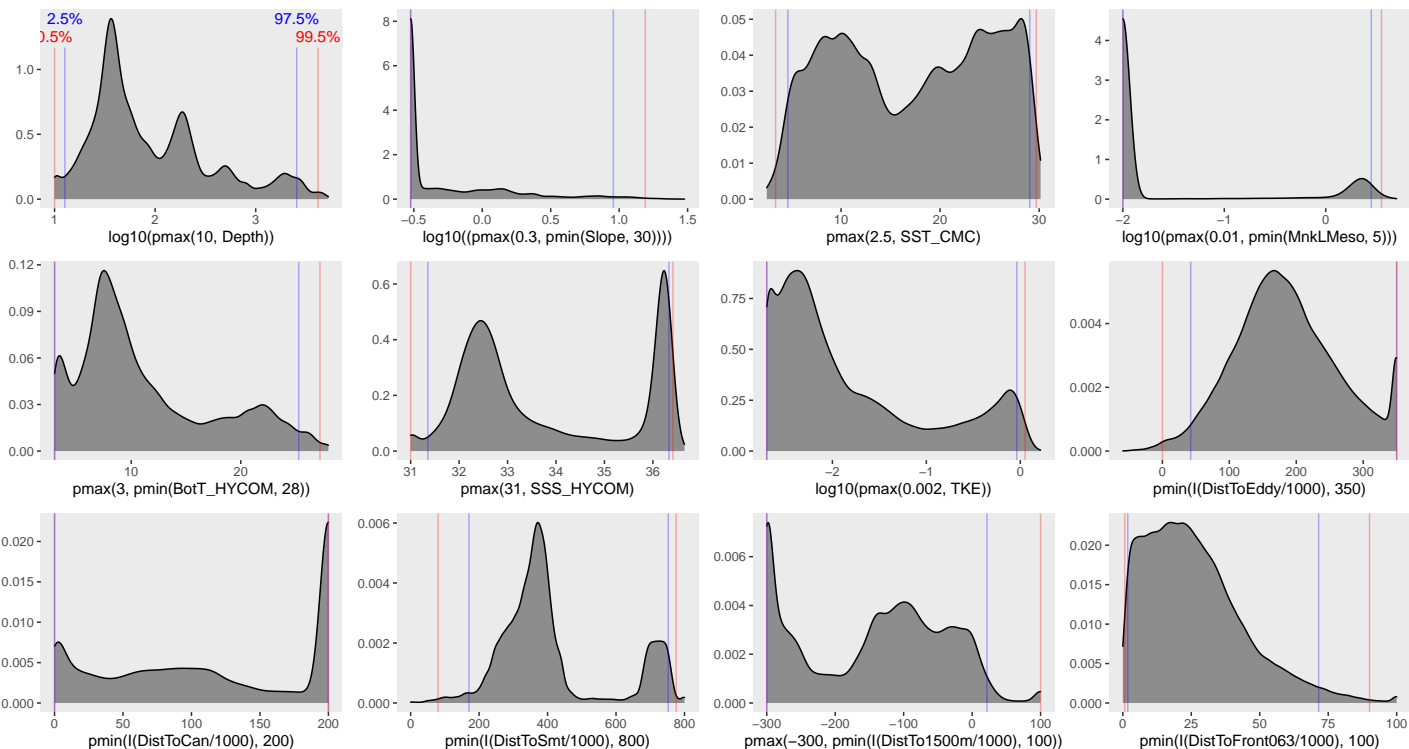


Figure 27: Density histograms showing the distributions of the covariates considered during the final model selection step. The final model may have included only a subset of the covariates shown here (see Figure 25), and additional covariates may have been considered in preceding selection steps. Red and blue lines enclose 99% and 95% of the distributions, respectively. Transforms and other treatments are indicated in axis labels.  $\log_{10}$  indicates the covariate was  $\log_{10}$  transformed.  $pmax$  and  $pmin$  indicate the covariate's minimum and maximum values, respectively, were Winsorized to the values shown. Winsorization was used to prevent runaway extrapolations during prediction when covariates exceeded sampled ranges, or for ecological reasons, depending on the covariate.  $/1000$  indicates meters were transformed to kilometers for interpretation convenience.

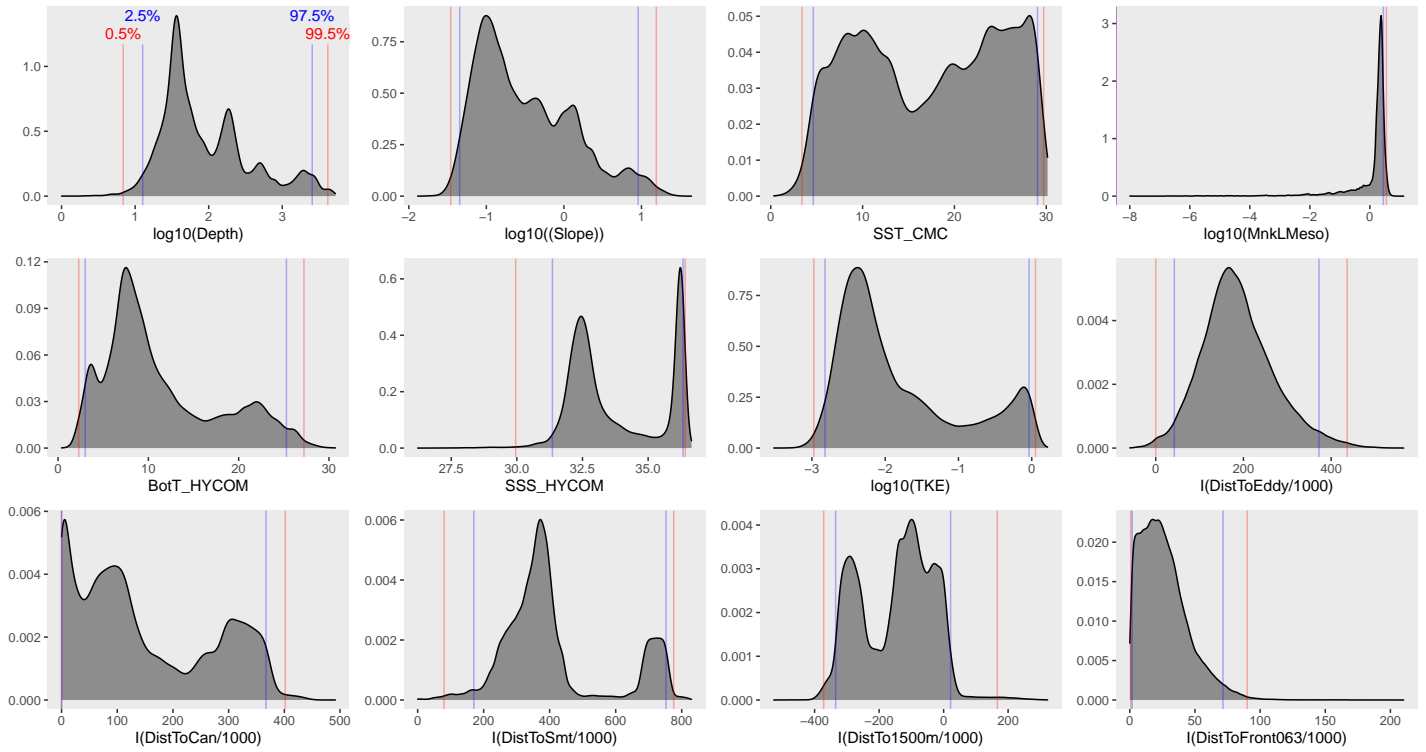


Figure 28: Density histograms shown in Figure 27 replotted without Winsorization, to show the full range of sampling represented by survey segments.

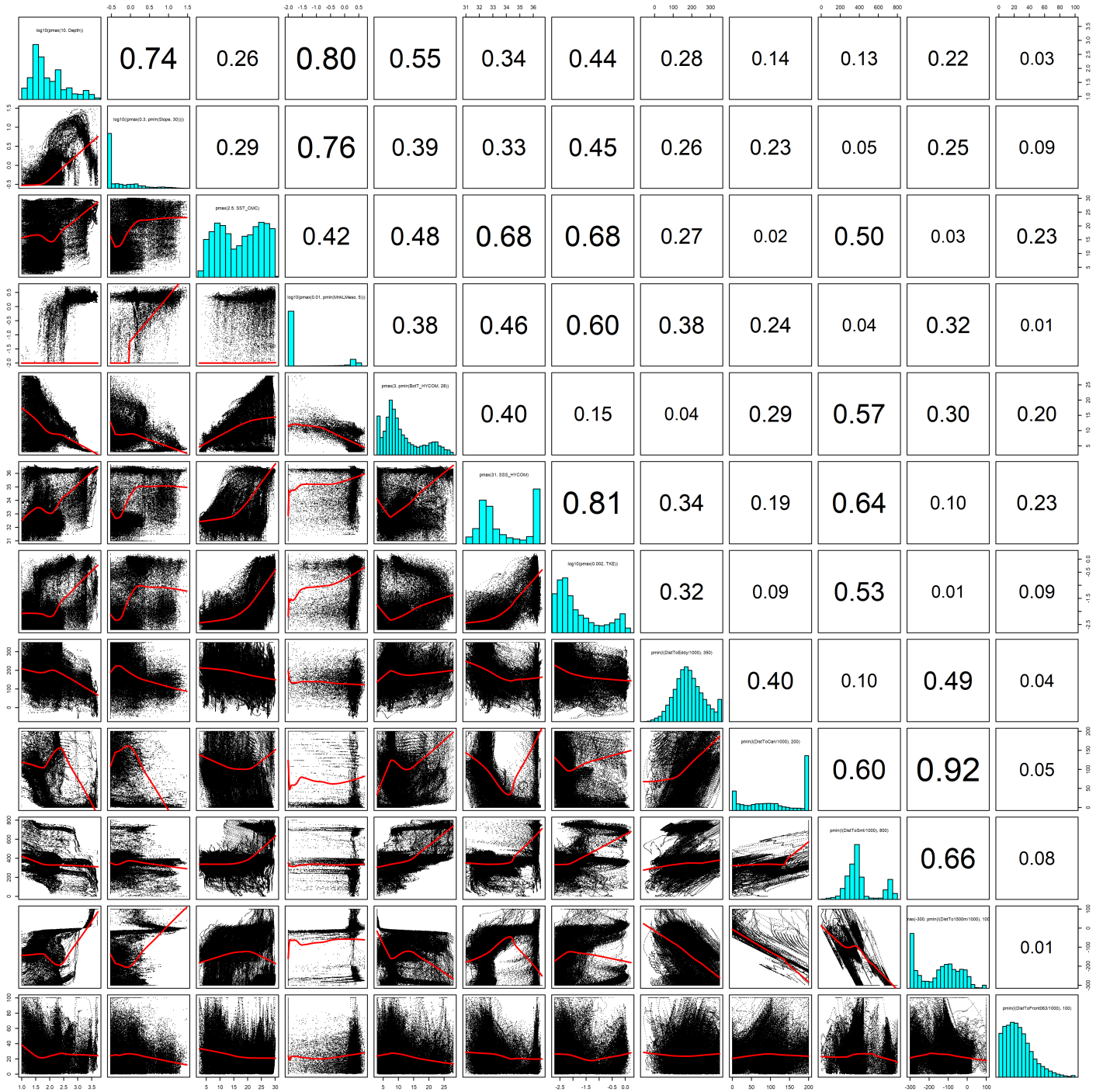


Figure 29: Scatterplot matrix of the covariates considered during the final model selection step. The final model may have included only a subset of the covariates shown here (see Figure 25), and additional covariates may have been considered in preceding selection steps. Covariates are transformed and Winsorized as shown in Figure 27. This plot is used to check simple correlations between covariates (via pairwise Pearson coefficients above the diagonal) and visually inspect for concurvity (via scatterplots and red lowess curves below the diagonal).

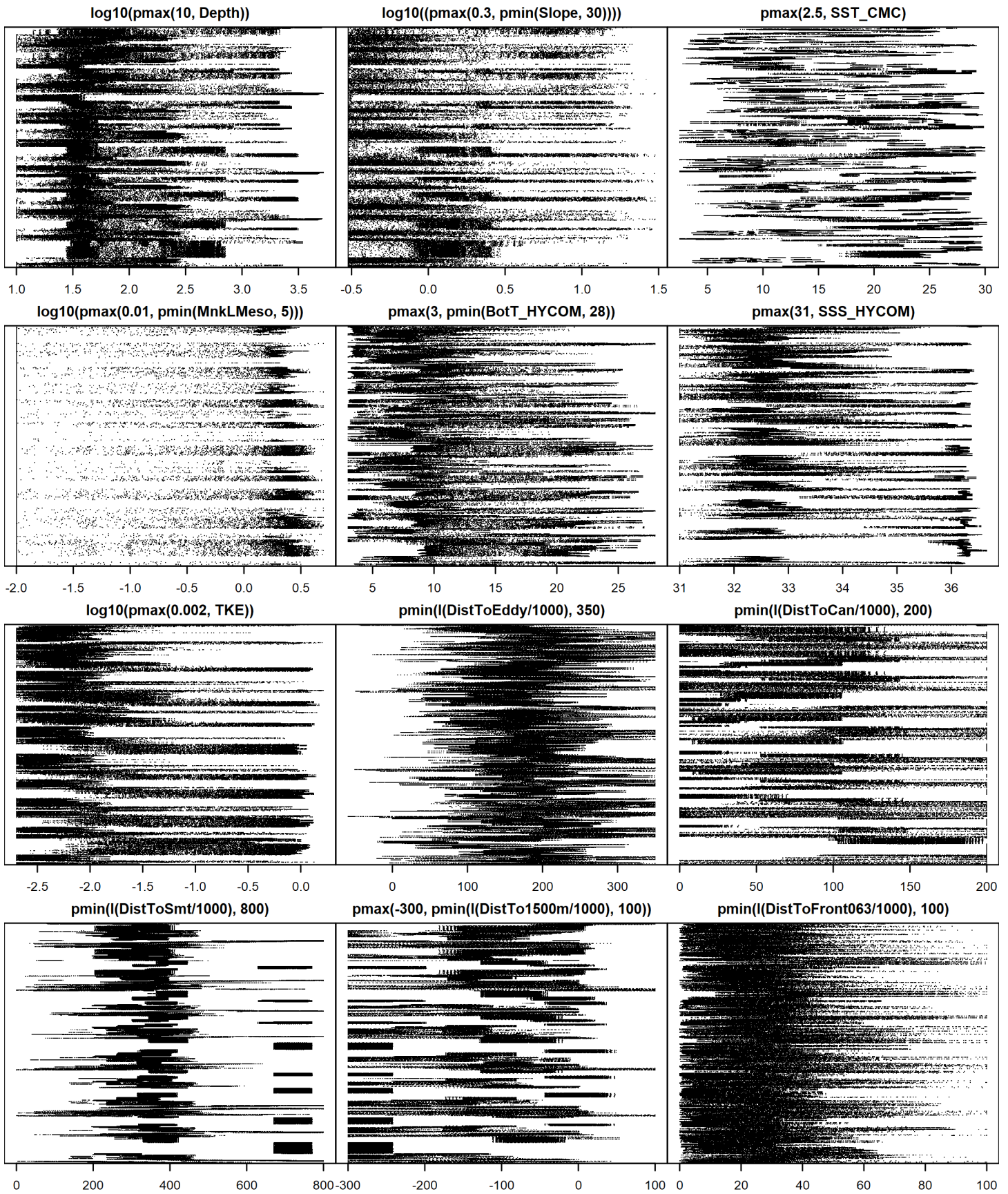


Figure 30: Dotplot of the covariates considered during the final model selection step. The final model may have included only a subset of the covariates shown here (see Figure 25), and additional covariates may have been considered in preceding selection steps. Covariates are transformed and Winsorized as shown in Figure 27. This plot is used to check for suspicious patterns and outliers in the data. Points are ordered vertically by segment ID, sequentially in time.

## 4.3 Extrapolation Diagnostics

### 4.3.1 Univariate Extrapolation

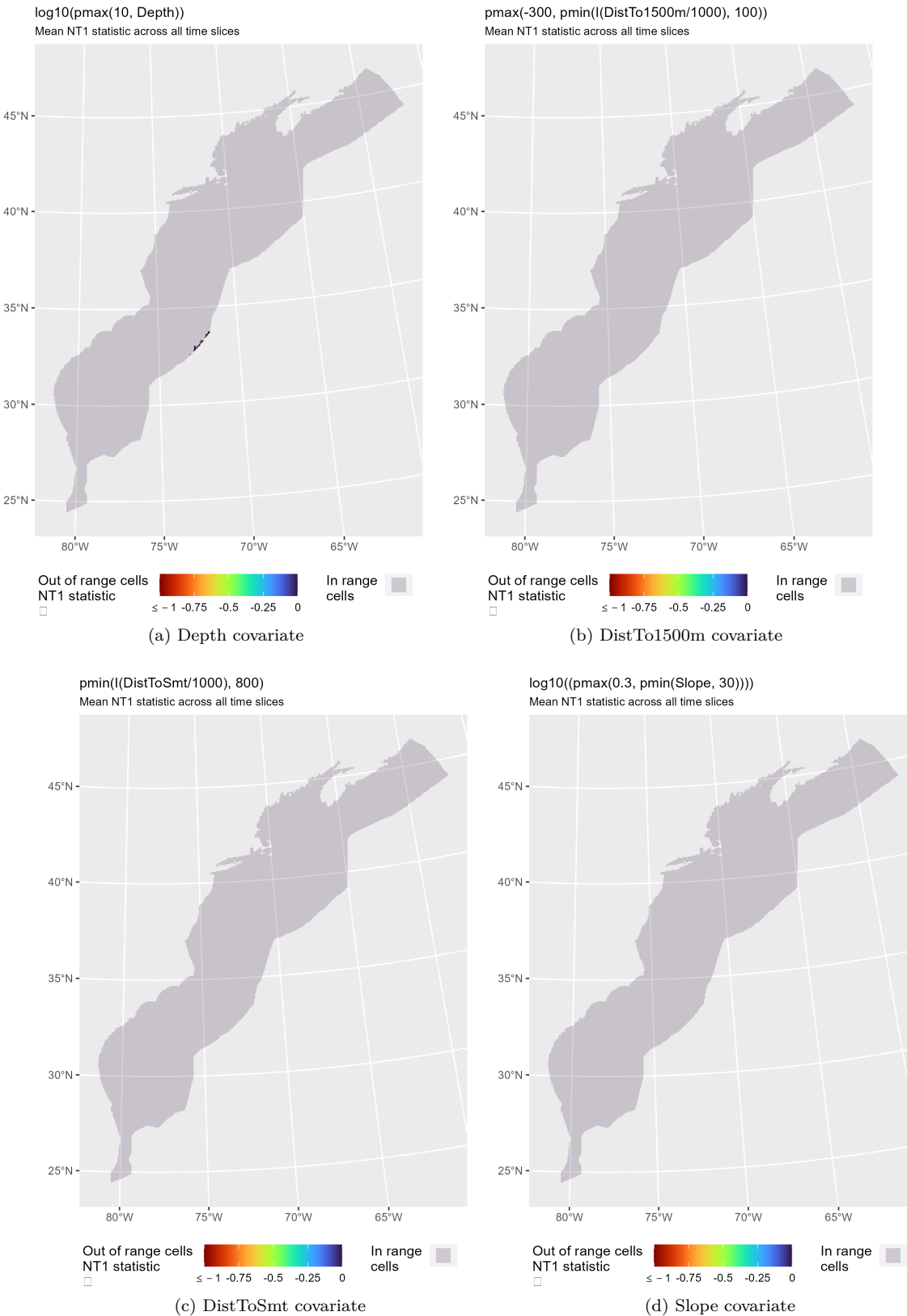


Figure 31: NT1 statistic (Mesgaran et al. (2014)) for static covariates used in the model. Areas outside the sampled range of a covariate appear in color, indicating univariate extrapolation of that covariate occurred there. Areas within the sampled range appear in gray, indicating it did not occur.



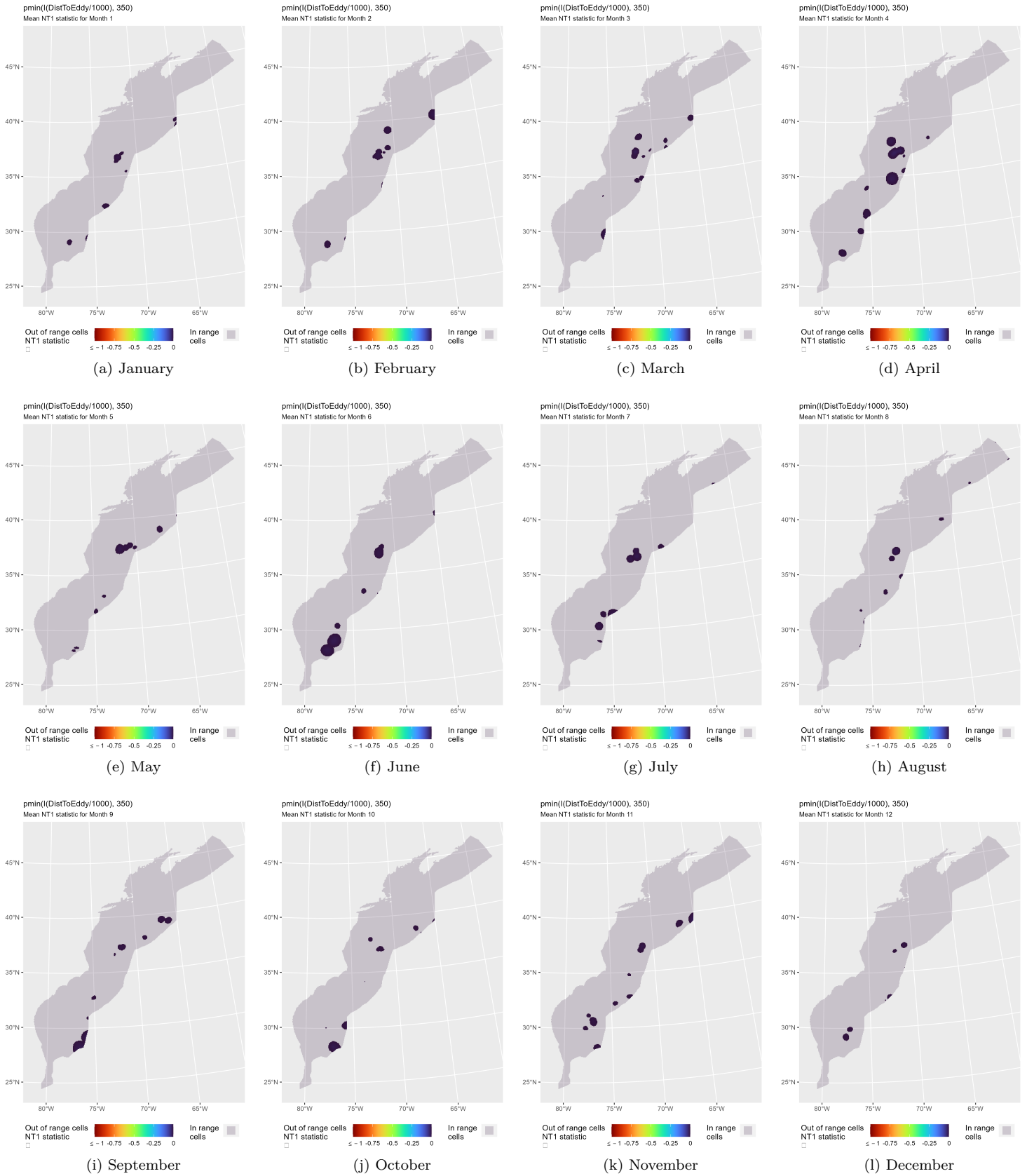


Figure 32: NT1 statistic (Mesgaran et al. (2014)) for the DistToEddy covariate in the model. Areas outside the sampled range of a covariate appear in color, indicating univariate extrapolation of that covariate occurred there during the month. Areas within the sampled range appear in gray, indicating it did not occur.

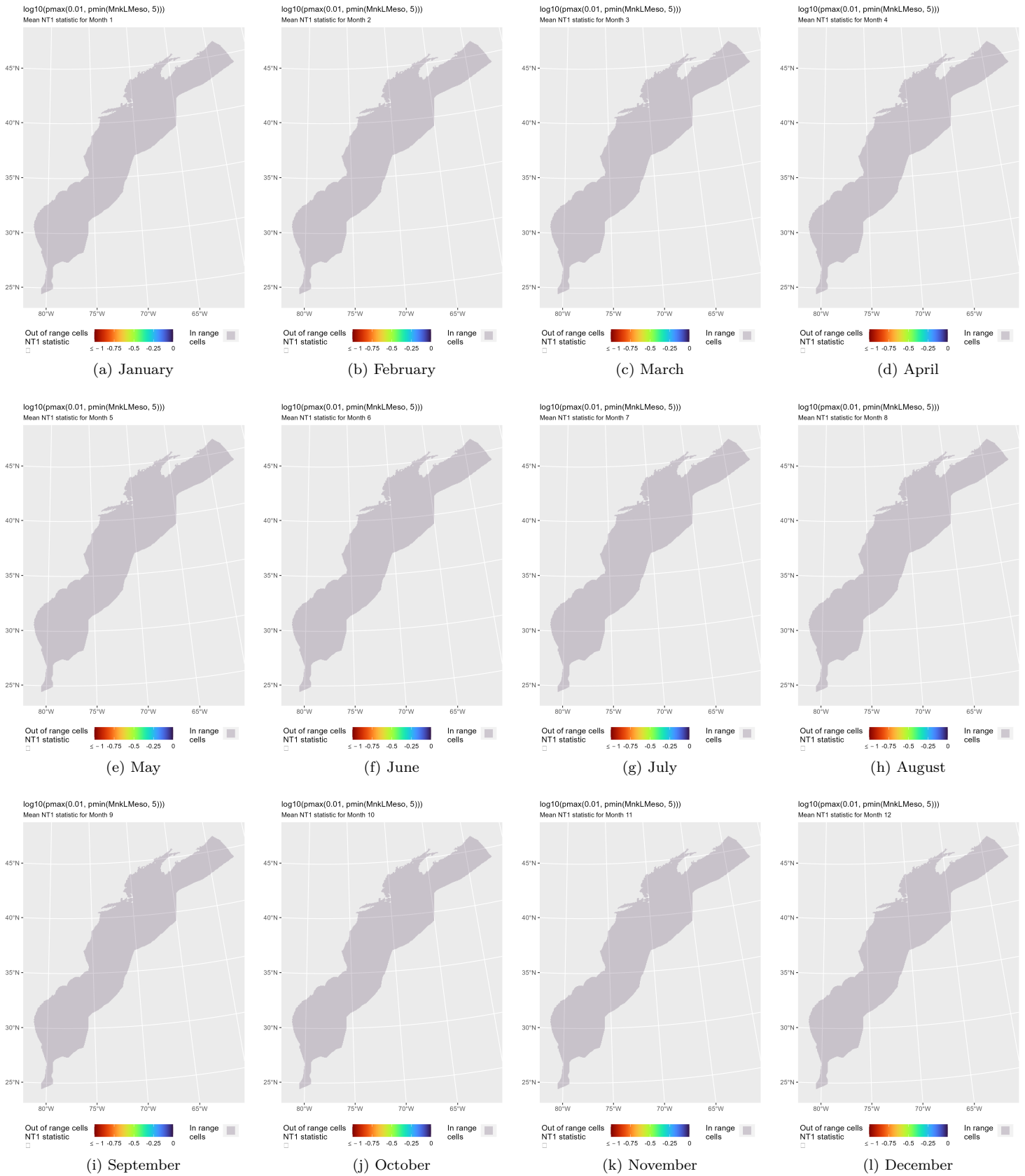


Figure 33: NT1 statistic (Mesgaran et al. (2014)) for the MnkLMeso covariate in the model. Areas outside the sampled range of a covariate appear in color, indicating univariate extrapolation of that covariate occurred there during the month. Areas within the sampled range appear in gray, indicating it did not occur.

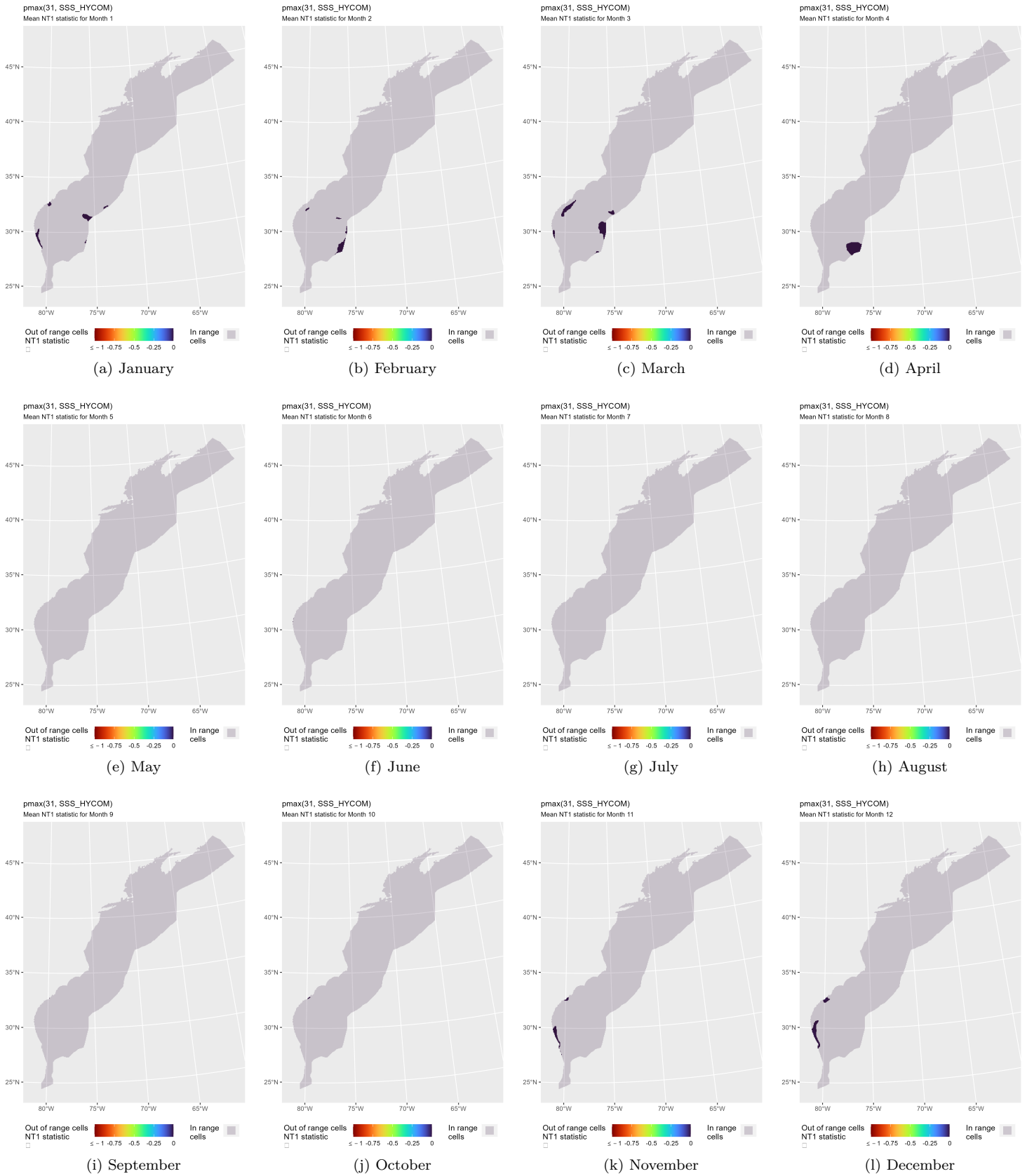


Figure 34: NT1 statistic (Mesgaran et al. (2014)) for the SSS\_HYCOM covariate in the model. Areas outside the sampled range of a covariate appear in color, indicating univariate extrapolation of that covariate occurred there during the month. Areas within the sampled range appear in gray, indicating it did not occur.

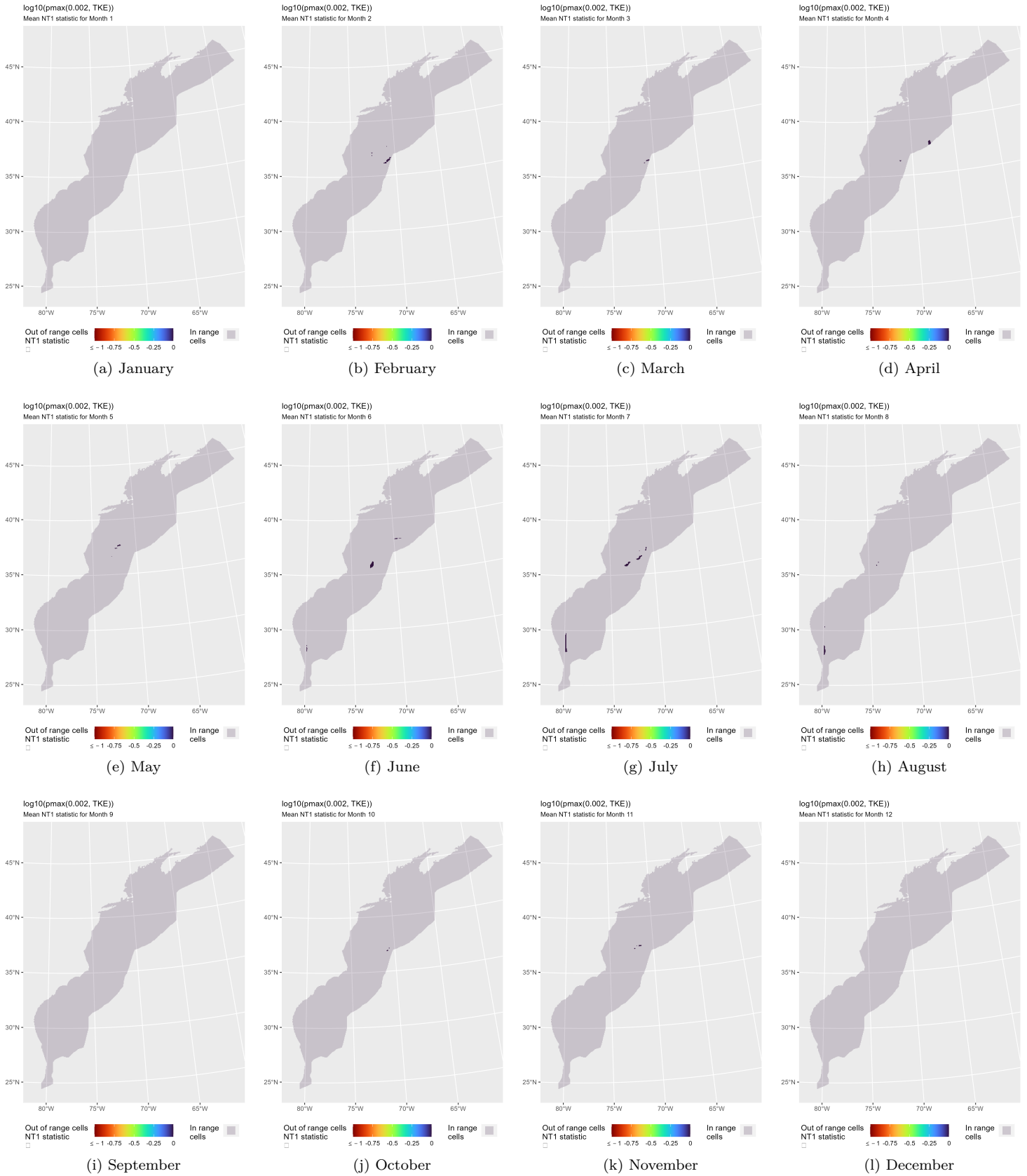


Figure 35: NT1 statistic (Mesgaran et al. (2014)) for the TKE covariate in the model. Areas outside the sampled range of a covariate appear in color, indicating univariate extrapolation of that covariate occurred there during the month. Areas within the sampled range appear in gray, indicating it did not occur.

### 4.3.2 Multivariate Extrapolation

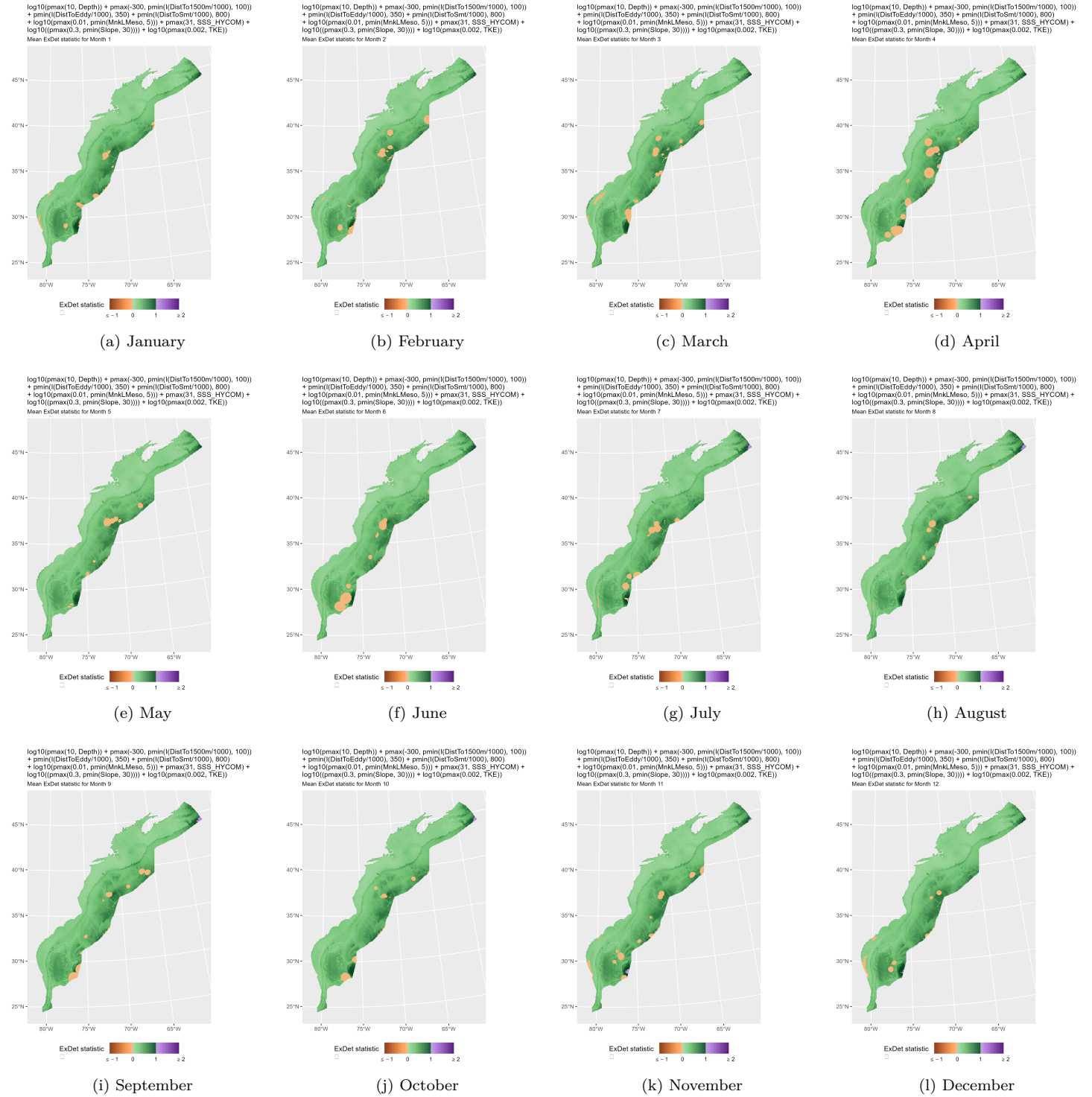


Figure 36: ExDet statistic (Mesgaran et al. (2014)) for all of the covariates used in the model. Areas in orange ( $\text{ExDet} < 0$ ) required univariate extrapolation of one or more covariates (see previous section). Areas in purple ( $\text{ExDet} > 1$ ), did not require univariate extrapolation but did require multivariate extrapolation, by virtue of having novel combinations of covariates not represented in the survey data, according to the NT2 statistic (Mesgaran et al. (2014)). Areas in green ( $0 \geq \text{ExDet} \leq 1$ ) did not require either type of extrapolation.

## 5 Predictions

Based on our evaluation of this model in the context of what is known of this species (see Section 4), we summarized its predictions into single, year-round climatological density and uncertainty surfaces (Figure 38). To illustrate the seasonal dynamics that result when predictions are summarized monthly instead, we included monthly mean abundances (Figure 37, Table 15), but to avoid confusion we did not include monthly maps in this report. They are available from us on request, but we recommend the year-round map be used for decision-making purposes, as discussed in Section 6.

### 5.1 Summarized Predictions

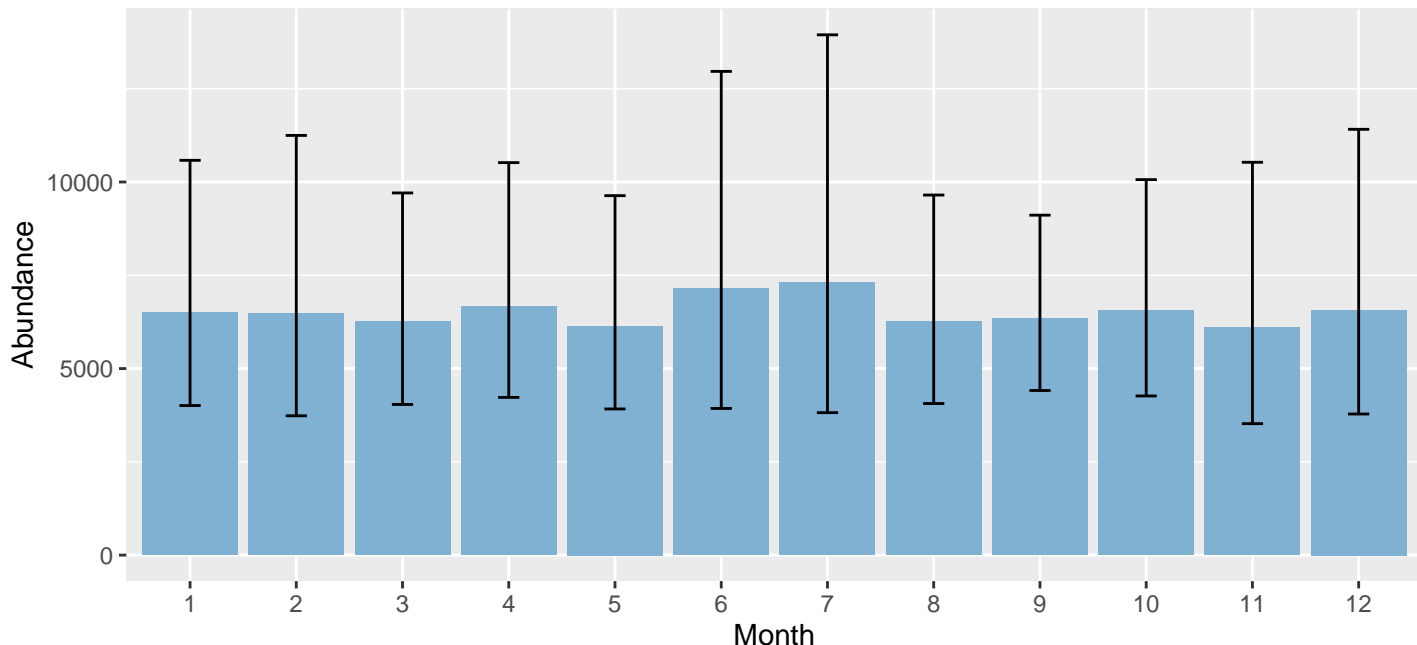


Figure 37: Mean monthly abundance for the prediction area for 2010-2019. Error bars are a 95% interval, made with a log-normal approximation using the prediction’s CV. The CV was estimated with the analytic approach given by Miller et al. (2022), Appendix S1, and accounts both for uncertainty in model parameter estimates and for temporal variability in dynamic covariates.

Table 15: Mean monthly abundance and density for the prediction area for 2010-2019. CV and intervals estimated as described for the previous figure.

Month	Abundance	CV	95% Interval	Area (km <sup>2</sup> )	Density (individuals / 100 km <sup>2</sup> )
1	6,513	0.251	4,008 - 10,581	1,272,925	0.512
2	6,481	0.287	3,734 - 11,248	1,272,925	0.509
3	6,260	0.227	4,038 - 9,707	1,272,925	0.492
4	6,669	0.236	4,227 - 10,520	1,272,925	0.524
5	6,143	0.233	3,917 - 9,634	1,272,925	0.483
6	7,139	0.312	3,932 - 12,965	1,272,925	0.561
7	7,297	0.340	3,818 - 13,944	1,272,925	0.573
8	6,261	0.223	4,063 - 9,650	1,272,925	0.492
9	6,340	0.187	4,412 - 9,112	1,272,925	0.498
10	6,552	0.222	4,266 - 10,064	1,272,925	0.515
11	6,091	0.285	3,523 - 10,529	1,272,925	0.478
12	6,570	0.287	3,782 - 11,413	1,272,925	0.516

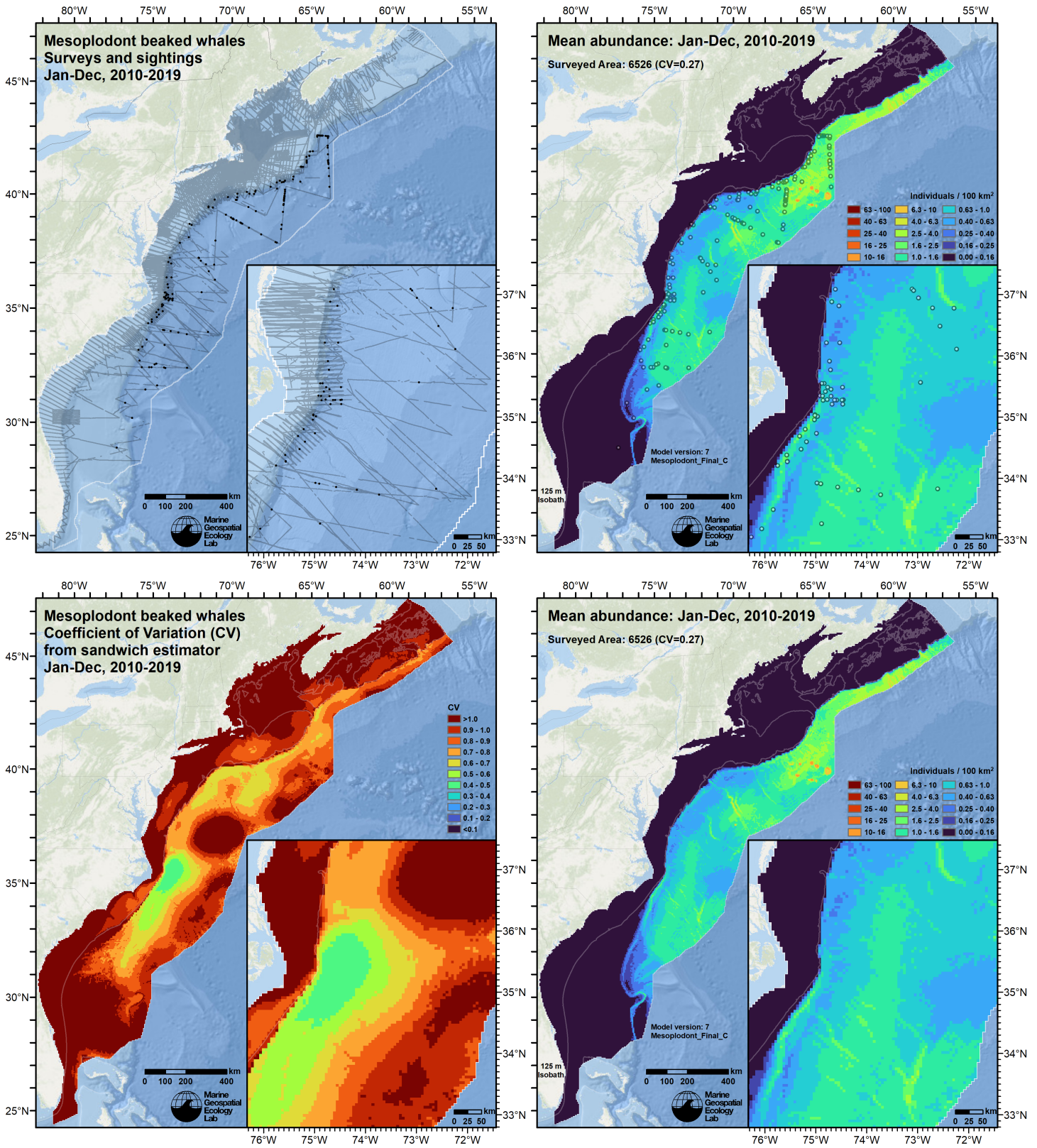


Figure 38: Survey effort and observations (top left), predicted density with observations (top right), predicted density without observations (bottom right), and coefficient of variation of predicted density (bottom left), for the given era. Variance was estimated with the analytic approach given by Miller et al. (2022), Appendix S1, and accounts both for uncertainty in model parameter estimates and for temporal variability in dynamic covariates.

## 5.2 Abundance Comparisons

### 5.2.1 NOAA Stock Assessment Report

Table 16: Comparison of regional abundance estimates from the 2019 NOAA Stock Assessment Report (SAR) (Hayes et al. (2020)) to estimates from this density model extracted from roughly comparable zones (Figure 39 below). The SAR estimates were based on a single year of surveying, while the model estimates were taken from the multi-year mean density surfaces we provide to model users (Section 5.1).

2021 Stock Assessment Report			Density Model		
Month/Year	Area	$N_{est}$	Period	Zone	Abundance
Jun-Sep 2016	Central Virginia to lower Bay of Fundy <sup>a</sup>	6,760	Year-Round 2010-2019	NEFSC	3,276
Jun-Aug 2016	Florida to central Virginia <sup>b</sup>	3,347	Year-Round 2010-2019	SEFSC	2,137
Jun-Aug 2016	Total	10,107	Year-Round 2010-2019	Total	5,413
	Bay of Fundy/Scotian Shelf		Year-Round 2010-2019	Canada <sup>c</sup>	1,060

<sup>a</sup> Estimate originally from Palka (2020).

<sup>b</sup> Estimate originally from Garrison (2020).

<sup>c</sup> Our Canada zone is roughly comparable to the SAR's Bay of Fundy/Scotian Shelf area (excluding the Gulf of St. Lawrence) however no estimates were provided by the SAR for this region.

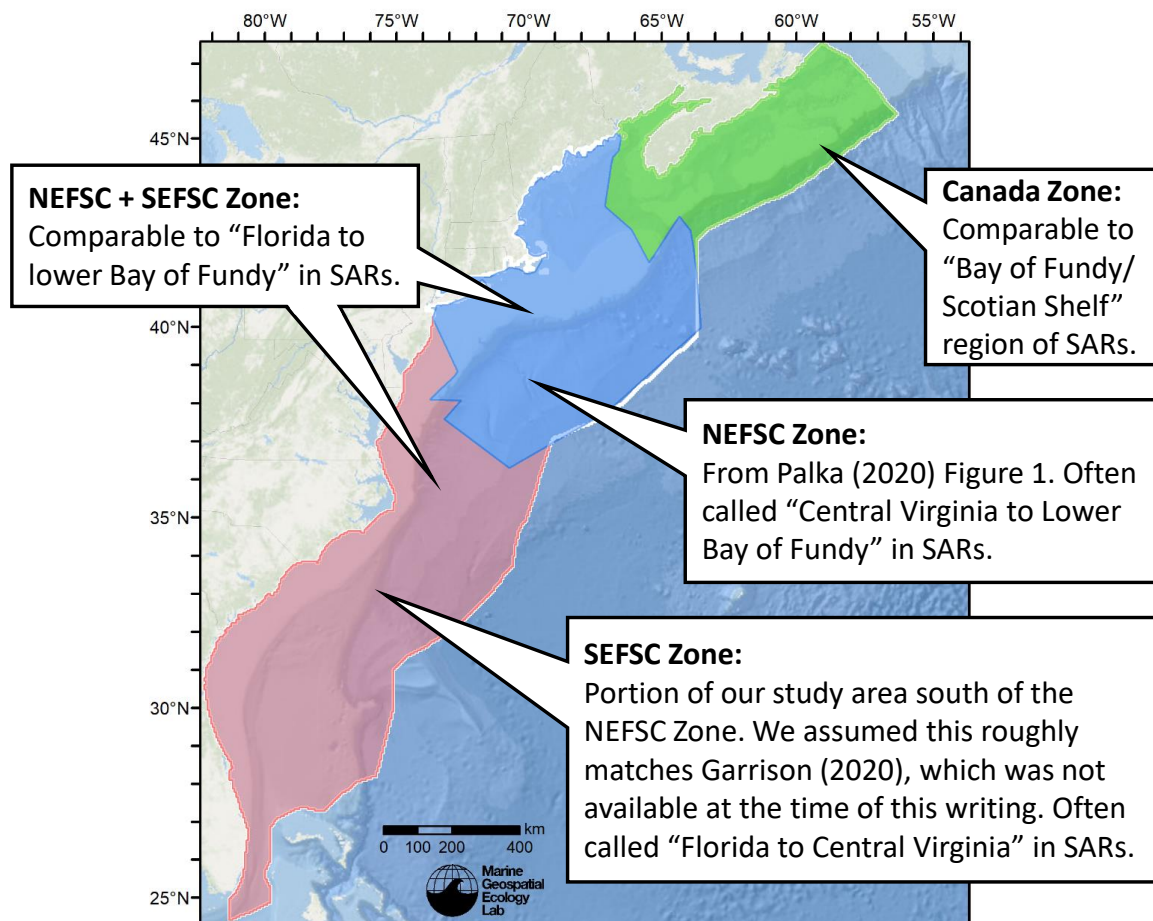


Figure 39: Zones for which we extracted abundance estimates from the density model for comparison to estimates from the NOAA Stock Assessment Report.



## 5.2.2 Previous Density Model

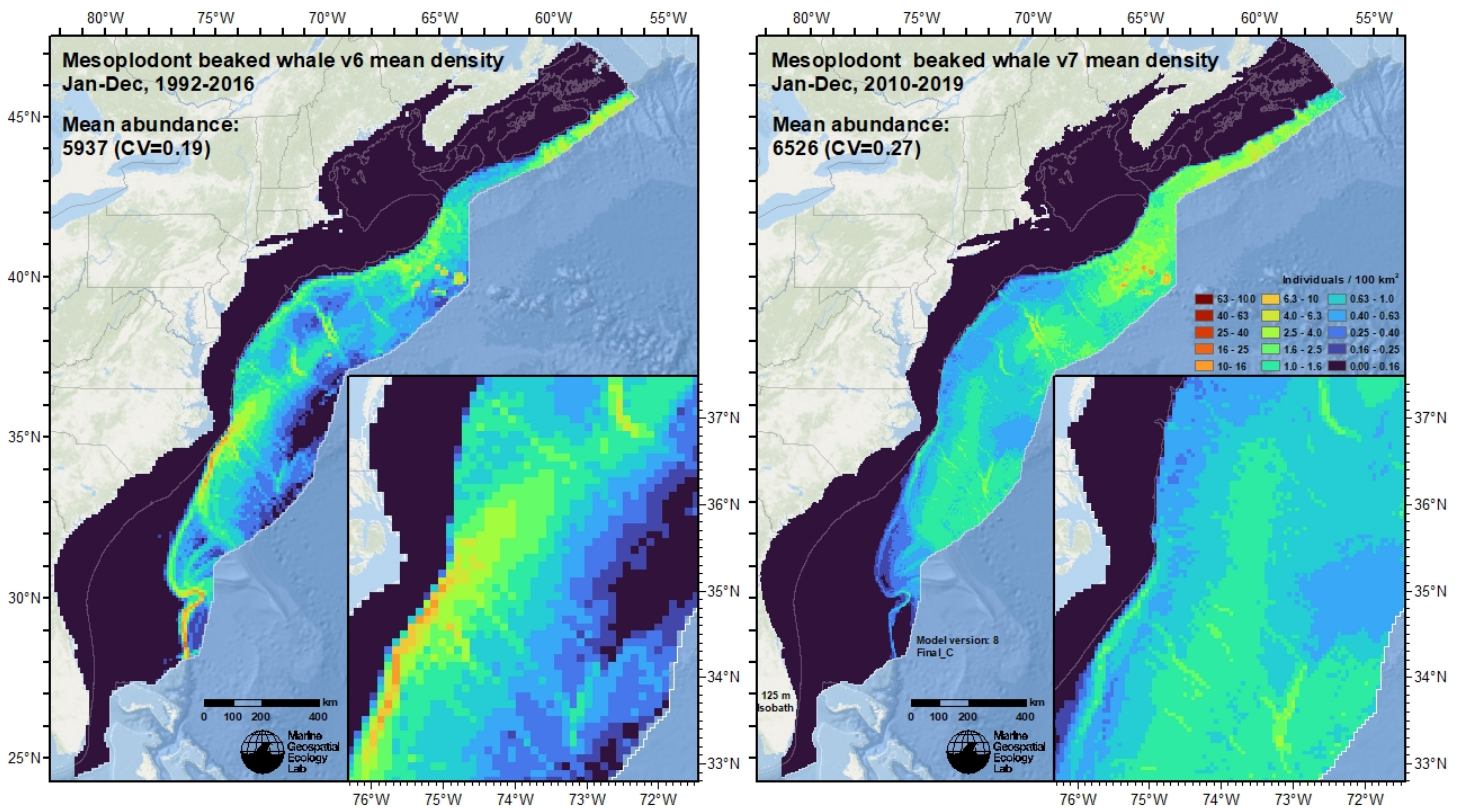


Figure 40: Comparison of the mean density predictions from the previous model (left) released by Roberts et al. (2017) to those from this model (right).

## 6 Discussion

The year-round mean abundance predicted is 6,526 Mesoplodonts with highest abundance predicted at the slope in the north and near seamounts. The model also shows abundance across the offshore regions, especially in the mid-Atlantic which was different from the Cuvier's beaked whale model. The monthly predictions showed that despite this being a contemporaneous model there was little change predicted monthly with a high of 7,297 animals predicted in July and a low of 6,091 predicted in November (Figure 37). This lent support to our decision to summarize density as a single, year-round surface for this species guild. It should be noted that these estimates are known to be biased low due to the fact that unidentified Ziphiidae abundance was also modeled and was estimated at 4,346 (CV=0.35) in the East Coast study area (see Unidentified beaked whale species report), and these numbers likely include an unknown number of Mesoplodont beaked whales.

The extrapolation statistics show some extrapolation in univariate space. Depth showed a few cells of extrapolated values at the eastern mid-Atlantic edge of the study area (Figure 31). The distance to eddy covariate showed some univariate extrapolation in all months (Figure 32). In this case distances “inside” the eddy ring are negative values, and the extrapolation cells indicate very large eddies, with large cores that are far from the ring in the negative direction. This is unlikely to be a major issue, as large eddies needed to trigger the extrapolation were infrequent and as such, unlikely to have yielded a big effect in the final model. Sea surface salinity showed swaths of out of range cells in the southwestern and southeastern edges of the study area in and around Blake Plateau in winter months and a few isolated out of range cells on the southwestern edge in spring (Figure 34). Finally, TKE showed a few out of range cells at the northern and southern edges of the Gulf Stream. (Figure 35).

In comparison to the SAR, our year-round mean abundance for the NEFSC region (3,276) was 52% lower than the SAR estimate (6,760). In the SEFSC region, the new model estimated 22% lower abundance (2,137) compared to the SAR estimate (3,347). This resulted in a combined year-round mean estimate (5,413) that was 46% lower than the SAR estimate (10,107). We recognize that these estimates are low compared to the SAR, perhaps due to differences in  $g(0)$  estimation and detection functions, or something particular to the 2016 survey year from which the SAR estimates were generated. We provided the year-round mean rather than monthlies, because no strong evidence of seasonal movement was indicated for these species. Additional surveying offshore in non-summer seasons is recommended to help elucidate seasonal variability.

In comparison to the Roberts et al. (2017) model, mean abundance was 9% higher in the new model. Abundance in the new model was more smoothed over the offshore regions with lower abundance predicted at the Blake Spur and off of Cape Hatteras. It is important to note that the new model was contemporaneous and the old model was climatological, as such there would be influence of seasonal variability on the year-round mean estimates in the new model that was absent in the old model.

As stated above, Mesoplodont beaked whales are a prime candidate for acoustic abundance estimation. Additionally, the acoustic data utilized in this modeling effort provided valuable information and allowed us to fill in critical knowledge gaps of Mesoplodont beaked whale occurrence in the mid-Atlantic offshore portion of the study area in winter and spring. We believe the addition of this data resulted in model improvement. Region-wide acoustic surveys targeting beaked whales as well as acoustic data from previous efforts in the North Atlantic (e.g. NOAA surveys) may be able to provide additional data for density surface modeling in future analysis and potentially allow for Mesoplodont beaked whales to be modeled at the species level if enough observations are available. Palka et al. (2021) reported only 0.4% of acoustic beaked whale detections as unidentified compared to 54% of visual beaked whale sightings during 2015-2016 surveys. This suggests that acoustic surveys for this species may provide better input to density surface models than visual surveys.

## References

- Baird RW, McSweeney DJ, Ligon AD, Webster DL (2004) Tagging Feasibility and Diving of Cuvier's Beaked Whales (*Ziphius cavirostris*) and Blainville's Beaked Whales (*Mesoplodon densirostris*) in Hawai'i.
- Barco SG, Burt L, DePerte A, Digiovanni R Jr. (2015) Marine Mammal and Sea Turtle Sightings in the Vicinity of the Maryland Wind Energy Area July 2013-June 2015, VAQF Scientific Report #2015-06. Virginia Aquarium & Marine Science Center Foundation, Virginia Beach, VA
- Barlow J (1999) Trackline detection probability for long-diving whales. In: Marine Mammal Survey and Assessment Methods. Balkema, Rotterdam, The Netherlands, pp 209–221
- Barlow J, Tyack PL, Johnson MP, Baird RW, Schorr GS, Andrews RD, Aguilar de Soto N (2013) Trackline and point detection probabilities for acoustic surveys of Cuvier's and Blainville's beaked whales. *The Journal of the Acoustical Society of America* 134:2486–2496. doi: [10.1121/1.4816573](https://doi.org/10.1121/1.4816573)
- Baumgartner MF (1997) The Distribution of Risso's Dolphin (*grampus Griseus*) with Respect to the Physiography of the Northern Gulf of Mexico. *Marine Mammal Science* 13:614–638. doi: [10.1111/j.1748-7692.1997.tb00087.x](https://doi.org/10.1111/j.1748-7692.1997.tb00087.x)
- Becker JJ, Sandwell DT, Smith WHF, Braud J, Binder B, Depner J, Fabre D, Factor J, Ingalls S, Kim S-H, Ladner R, Marks K, Nelson S, Pharaoh A, Trimmer R, Von Rosenberg J, Wallace G, Weatherall P (2009) Global Bathymetry and Elevation Data at 30 Arc Seconds Resolution: SRTM30\_PLUS. *Marine Geodesy* 32:355–371. doi: [10.1080/01490410903297766](https://doi.org/10.1080/01490410903297766)
- Boisseau O, Nowacek D, Roberts J, Pabst DA, Clabaugh A, Moscrop A, McLanaghan R, Yack T, Levenson JJ (in review) Acoustic density estimates of beaked whales off the mid-Atlantic coast of the USA in winter and spring.
- Buckland ST, Anderson DR, Burnham KP, Laake JL, Borchers DL, Thomas L (2001) *Introduction to Distance Sampling: Estimating Abundance of Biological Populations*. Oxford University Press, Oxford, UK
- Burt ML, Borchers DL, Jenkins KJ, Marques TA (2014) Using mark-recapture distance sampling methods on line transect surveys. *Methods in Ecology and Evolution* 5:1180–1191. doi: [10.1111/2041-210X.12294](https://doi.org/10.1111/2041-210X.12294)
- Chassignet E, Hurlburt H, Metzger EJ, Smedstad O, Cummings J, Halliwell G, Bleck R, Baraille R, Wallcraft A, Lozano C, Tolman H, Srinivasan A, Hankin S, Cornillon P, Weisberg R, Barth A, He R, Werner F, Wilkin J (2009) US GODAE: Global Ocean Prediction with the HYbrid Coordinate Ocean Model (HYCOM). *Oceanog* 22:64–75. doi: [10.5670/oceanog.2009.39](https://doi.org/10.5670/oceanog.2009.39)
- Chelton DB, Schlax MG, Samelson RM (2011) Global observations of nonlinear mesoscale eddies. *Progress in Oceanography* 91:167–216. doi: [10.1016/j.pocean.2011.01.002](https://doi.org/10.1016/j.pocean.2011.01.002)
- Cohen RE, Frasier KE, Baumann-Pickering S, Wiggins SM, Rafter MA, Baggett LM, Hildebrand JA (2022) Identification of western North Atlantic odontocete echolocation click types using machine learning and spatiotemporal correlates. *PLoS ONE* 17:e0264988. doi: [10.1371/journal.pone.0264988](https://doi.org/10.1371/journal.pone.0264988)
- Cole T, Gerrior P, Merrick RL (2007) [Methodologies of the NOAA National Marine Fisheries Service Aerial Survey Program for Right Whales \(\*Eubalaena glacialis\*\) in the Northeast U.S., 1998-2006](#). U.S. Department of Commerce, Woods Hole, MA
- Cotter MP (2019) *Aerial Surveys for Protected Marine Species in the Norfolk Canyon Region: 2018–2019 Final Report*. HDR, Inc., Virginia Beach, VA

- Foley HJ, Paxton CGM, McAlarney RJ, Pabst DA, Read AJ (2019) Occurrence, Distribution, and Density of Protected Species in the Jacksonville, Florida, Atlantic Fleet Training and Testing (AFTT) Study Area. Duke University Marine Lab, Beaufort, NC
- Garrison LP (2020) [Abundance of cetaceans along the southeast U.S. East coast from a summer 2016 vessel survey](#). PRD Contribution # PRD-2020-04. NOAA National Marine Fisheries Service, Southeast Fisheries Science Center, Miami, FL
- Hamazaki T (2002) [Spatiotemporal prediction models of cetacean habitats in the mid-western North Atlantic ocean \(from Cape Hatteras, North Carolina, USA to Nova Scotia, Canada\)](#). Marine Mammal Science 18:920–939.
- Harris PT, Macmillan-Lawler M, Rupp J, Baker EK (2014) Geomorphology of the oceans. Marine Geology 352:4–24. doi: [10.1016/j.margeo.2014.01.011](#)
- Hayes SA, Josephson E, Maze-Foley K, Rosel PE, Byrd B, Chavez-Rosales S, Cole TV, Garrison LP, Hatch J, Henry A, Horstman SC, Litz J, Lyssikatos MC, Mullin KD, Orphanides C, Pace RM, Palka DL, Powell J, Wenzel FW (2020) [US Atlantic and Gulf of Mexico Marine Mammal Stock Assessments - 2019](#). NOAA National Marine Fisheries Service, Northeast Fisheries Science Center, Woods Hole, MA
- Jefferson T, Webber M, RL P (2008) Marine mammals of the world. Burlington, MA.
- Laake JL, Calambokidis J, Osmek SD, Rugh DJ (1997) Probability of Detecting Harbor Porpoise From Aerial Surveys: Estimating  $g(0)$ . Journal of Wildlife Management 61:63–75. doi: [10.2307/3802415](#)
- Lehodey P, Senina I, Murtugudde R (2008) A spatial ecosystem and populations dynamics model (SEAPODYM)–Modeling of tuna and tuna-like populations. Progress in Oceanography 78:304–318. doi: [10.1016/j.pocean.2008.06.004](#)
- Lehodey P, Conchon A, Senina I, Domokos R, Calmettes B, Jouanno J, Hernandez O, Kloster R (2015) Optimization of a micronekton model with acoustic data. ICES Journal of Marine Science 72:1399–1412. doi: [10.1093/icesjms/fsu233](#)
- Leiter S, Stone K, Thompson J, Accardo C, Wikgren B, Zani M, Cole T, Kenney R, Mayo C, Kraus S (2017) North Atlantic right whale *Eubalaena glacialis* occurrence in offshore wind energy areas near Massachusetts and Rhode Island, USA. Endang Species Res 34:45–59. doi: [10.3354/esr00827](#)
- MacLeod CD, Zuur AF (2005) [Habitat utilization by Blainville’s beaked whales off Great Abaco, northern Bahamas, in relation to seabed topography](#). Marine Biology 147:1–11.
- MacLeod CD, Perrin WF, Pitman R, Barlow J, Ballance L, D’Amico A, Gerrodette T, Joyce G, Mullin KD, Palka DL, others (2005) [Known and inferred distributions of beaked whale species \(Cetacea: Ziphiidae\)](#). Journal of Cetacean Research and Management 7:271.
- MacLeod CD, Perrin WF, Pitman R, Barlow J, Ballance L, D’Amico A, Gerrodette T, Joyce G, Mullin KD, Palka DL, Waring GT (2006) Known and inferred distributions of beaked whale species (Cetacea: Ziphiidae). 16.
- Mallette SD, Lockhart GG, McAlarney RJ, Cummings EW, McLellan WA, Pabst DA, Barco SG (2014) Documenting Whale Migration off Virginia’s Coast for Use in Marine Spatial Planning: Aerial and Vessel Surveys in the Proximity of the Virginia Wind Energy Area (VA WEA), VAQF Scientific Report 2014-08. Virginia Aquarium & Marine Science Center Foundation, Virginia Beach, VA
- Mallette SD, Lockhart GG, McAlarney RJ, Cummings EW, McLellan WA, Pabst DA, Barco SG (2015) Documenting Whale Migration off Virginia’s Coast for Use in Marine Spatial Planning: Aerial Surveys in the Proximity of the Virginia Wind Energy Area (VA WEA) Survey/Reporting Period: May 2014 - December 2014, VAQF Scientific Report 2015-02. Virginia Aquarium & Marine Science Center Foundation, Virginia Beach, VA
- Mallette SD, McAlarney RJ, Lockhart GG, Cummings EW, Pabst DA, McLellan WA, Barco SG (2017) [Aerial Survey Baseline Monitoring in the Continental Shelf Region of the VACAPES OPAREA: 2016 Annual Progress Report](#). Virginia Aquarium & Marine Science Center Foundation, Virginia Beach, VA
- Marsh H, Sinclair DF (1989) Correcting for Visibility Bias in Strip Transect Aerial Surveys of Aquatic Fauna. The Journal of Wildlife Management 53:1017. doi: [10.2307/3809604](#)
- McAlarney R, Cummings E, McLellan W, Pabst A (2018) Aerial Surveys for Protected Marine Species in the Norfolk Canyon Region: 2017 Annual Progress Report. University of North Carolina Wilmington, Wilmington, NC
- McLellan WA, McAlarney RJ, Cummings EW, Read AJ, Paxton CGM, Bell JT, Pabst DA (2018) Distribution and abundance of beaked whales (Family Ziphiidae) Off Cape Hatteras, North Carolina, U.S.A. Marine Mammal Science. doi: [10.1111/mms.12500](#)
- Mead JG (1989) Bottlenose whales. In: Handbook of marine mammals, Sam H. Ridgway and Sir Richard Harrison. Academic Press, pp 321–348

- Mesgaran MB, Cousens RD, Webber BL (2014) Here be dragons: A tool for quantifying novelty due to covariate range and correlation change when projecting species distribution models. *Diversity Distrib* 20:1147–1159. doi: [10.1111/ddi.12209](https://doi.org/10.1111/ddi.12209)
- Miller DL, Becker EA, Forney KA, Roberts JJ, Cañadas A, Schick RS (2022) Estimating uncertainty in density surface models. *PeerJ* 10:e13950. doi: [10.7717/peerj.13950](https://doi.org/10.7717/peerj.13950)
- Moulins A, Rosso M, Nani B, Würtz M (2007) Aspects of the distribution of Cuvier's beaked whale (*Ziphius Cavirostris*) in relation to topographic features in the *Pelagos Sanctuary* (north-western Mediterranean Sea). *J Mar Biol Ass* 87:177–186. doi: [10.1017/S0025315407055002](https://doi.org/10.1017/S0025315407055002)
- O'Brien O, Pendleton DE, Ganley LC, McKenna KR, Kenney RD, Quintana-Rizzo E, Mayo CA, Kraus SD, Redfern JV (2022) Repatriation of a historical North Atlantic right whale habitat during an era of rapid climate change. *Sci Rep* 12:12407. doi: [10.1038/s41598-022-16200-8](https://doi.org/10.1038/s41598-022-16200-8)
- Palka D (2020) [Cetacean Abundance in the US Northwestern Atlantic Ocean Summer 2016](#). *Northeast Fish Sci Cent Ref Doc. 20-05*. NOAA National Marine Fisheries Service, Northeast Fisheries Science Center, Woods Hole, MA
- Palka D, Aichinger Dias L, Broughton E, Chavez-Rosales S, Cholewiak D, Davis G, DeAngelis A, Garrison L, Haas H, Hatch J, Hyde K, Jech M, Josephson E, Mueller-Brennan L, Orphanides C, Pegg N, Sasso C, Sigourney D, Soldevilla M, Walsh H (2021) [Atlantic Marine Assessment Program for Protected Species: FY15 – FY19 \(OCS Study BOEM 2021-051\)](#). U.S. Department of the Interior, Bureau of Ocean Energy Management, Washington, DC
- Palka DL (2006) [Summer abundance estimates of cetaceans in US North Atlantic navy operating areas \(NEFSC Reference Document 06-03\)](#). U.S. Department of Commerce, Northeast Fisheries Science Center, Woods Hole, MA
- Palka DL, Chavez-Rosales S, Josephson E, Cholewiak D, Haas HL, Garrison L, Jones M, Sigourney D, Waring G, Jech M, Broughton E, Soldevilla M, Davis G, DeAngelis A, Sasso CR, Winton MV, Smolowitz RJ, Fay G, LaBrecque E, Leiness JB, Dettloff K, Warden M, Murray K, Orphanides C (2017) [Atlantic Marine Assessment Program for Protected Species: 2010-2014 \(OCS Study BOEM 2017-071\)](#). U.S. Department of the Interior, Bureau of Ocean Energy Management, Washington, DC
- Quintana-Rizzo E, Leiter S, Cole T, Hagbloom M, Knowlton A, Nagelkirk P, O'Brien O, Khan C, Henry A, Duley P, Crowe L, Mayo C, Kraus S (2021) Residency, demographics, and movement patterns of North Atlantic right whales *Eubalaena glacialis* in an offshore wind energy development area in southern New England, USA. *Endang Species Res* 45:251–268. doi: [10.3354/esr01137](https://doi.org/10.3354/esr01137)
- Read AJ, Barco S, Bell J, Borchers DL, Burt ML, Cummings EW, Dunn J, Fougères EM, Hazen L, Hodge LEW, Laura A-M, McAlarney RJ, Peter N, Pabst DA, Paxton CGM, Schneider SZ, Urian KW, Waples DM, McLellan WA (2014) [Occurrence, distribution and abundance of cetaceans in Onslow Bay, North Carolina, USA](#). *Journal of Cetacean Research and Management* 14:23–35.
- Redfern JV, Kryc KA, Weiss L, Hodge BC, O'Brien O, Kraus SD, Quintana-Rizzo E, Auster PJ (2021) Opening a Marine Monument to Commercial Fishing Compromises Species Protections. *Front Mar Sci* 8:645314. doi: [10.3389/fmars.2021.645314](https://doi.org/10.3389/fmars.2021.645314)
- Roberts JJ, Best BD, Dunn DC, Treml EA, Halpin PN (2010) Marine Geospatial Ecology Tools: An integrated framework for ecological geoprocessing with ArcGIS, Python, R, MATLAB, and C++. *Environmental Modelling & Software* 25:1197–1207. doi: [10.1016/j.envsoft.2010.03.029](https://doi.org/10.1016/j.envsoft.2010.03.029)
- Roberts JJ, Best BD, Mannocci L, Fujioka E, Halpin PN, Palka DL, Garrison LP, Mullin KD, Cole TVN, Khan CB, McLellan WA, Pabst DA, Lockhart GG (2016) Habitat-based cetacean density models for the U.S. Atlantic and Gulf of Mexico. *Scientific Reports* 6:22615. doi: [10.1038/srep22615](https://doi.org/10.1038/srep22615)
- Roberts JJ, Mannocci L, Halpin PN (2017) Final Project Report: Marine Species Density Data Gap Assessments and Update for the AFTT Study Area, 2016-2017 (Opt. Year 1), Document Version 1.4. Duke University Marine Geospatial Ecology Lab, Durham, NC
- Roberts JJ, Yack TM, Halpin PN (2023) Marine mammal density models for the U.S. Navy Atlantic Fleet Training and Testing (AFTT) study area for the Phase IV Navy Marine Species Density Database (NMSDD), Document Version 1.3. Duke University Marine Geospatial Ecology Lab, Durham, NC
- Robertson FC, Koski WR, Brandon JR, Thomas TA, Trites AW (2015) [Correction factors account for the availability of bowhead whales exposed to seismic operations in the Beaufort Sea](#). *Journal of Cetacean Research and Management* 15:35–44.
- Schlx MG, Chelton DB (2016) [The "Growing Method" of Eddy Identification and Tracking in Two and Three Dimensions](#). College of Earth, Ocean and Atmospheric Sciences, Oregon State University, Corvallis, OR
- Seber GAF, others (1982) The estimation of animal abundance and related parameters.

- Shearer JM, Quick NJ, Cioffi WR, Baird RW, Webster DL, Foley HJ, Swaim ZT, Waples DM, Bell JT, Read AJ (2019) Diving behaviour of Cuvier's beaked whales ( *Ziphius Cavirostris* ) off Cape Hatteras, North Carolina. Royal Society Open Science 6:181728. doi: [10.1098/rsos.181728](https://doi.org/10.1098/rsos.181728)
- Stanistreet JE, Nowacek DP, Baumann-Pickering S, Bell JT, Cholewiak DM, Hildebrand JA, Hodge LEW, Moors-Murphy HB, Van Parijs SM, Read AJ (2017) Using passive acoustic monitoring to document the distribution of beaked whale species in the western North Atlantic Ocean. Canadian Journal of Fisheries and Aquatic Sciences 1–12. doi: [10.1139/cjfas-2016-0503](https://doi.org/10.1139/cjfas-2016-0503)
- Stone KM, Leiter SM, Kenney RD, Wikgren BC, Thompson JL, Taylor JKD, Kraus SD (2017) Distribution and abundance of cetaceans in a wind energy development area offshore of Massachusetts and Rhode Island. J Coast Conserv 21:527–543. doi: [10.1007/s11852-017-0526-4](https://doi.org/10.1007/s11852-017-0526-4)
- Tove M (1995) LIVE SIGHTING OF MESOPLODON CF. M. MIRUS, TRUE'S BEAKED WHALE. Marine Mammal Sci 11:80–85. doi: [10.1111/j.1748-7692.1995.tb00276.x](https://doi.org/10.1111/j.1748-7692.1995.tb00276.x)
- Tyack PL, Johnson M, Soto NA, Sturlese A, Madsen PT (2006) Extreme diving of beaked whales. Journal of Experimental Biology 209:4238–4253. doi: [10.1242/jeb.02505](https://doi.org/10.1242/jeb.02505)
- Waring GT, Hamazaki T, Sheehan D, Wood G, Baker S (2001) [Characterization of beaked whale \(Ziphiidae\) and sperm whale \(Physeter macrocephalus\) summer habitat in shelf-edge and deeper waters off the northeast US](#). Marine Mammal Science 17:703–717.
- Zoidis AM, Lomac-MacNair KS, Ireland DS, Rickard ME, McKown KA, Schlesinger MD (2021) Distribution and density of six large whale species in the New York Bight from monthly aerial surveys 2017 to 2020. Continental Shelf Research 230:104572. doi: [10.1016/j.csr.2021.104572](https://doi.org/10.1016/j.csr.2021.104572)